AD-A108 268 NEW MEXICO ENGINEERING RESEARCH INST ALBUQUERQUE F/G 18/3
CYLINDRICAL IN SITU TESTS (CIST) 20 AND 21: ANALYSIS REPORT.(U)
AUG 81 J D SHINN, J BEAN F29601-76-C-0015
UNCLASSIFIED NMERI-DP/EM-34 AFWL-TR-80-152 NL

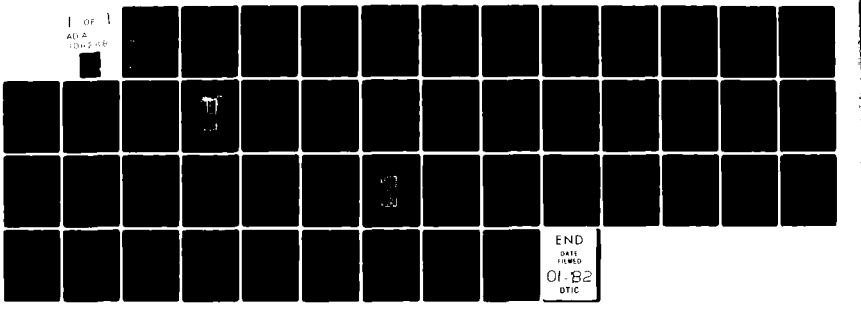

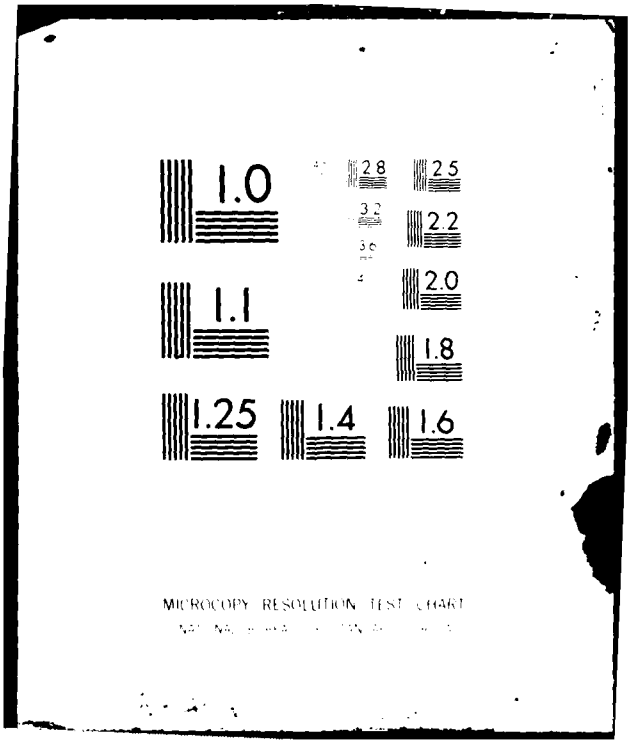
1.0
2.8
2.5
3.2
2.2
3.6
2.0
1.1
1.8
1.25
1.4
1.6
MICROCOPY RESOLUTION TEST CHART

AFWL-TR-80-152

(12) LEVEL II

AFWL-TR-80-152

AD A108268

# CYLINDRICAL IN SITU TESTS (CIST) 20 AND 21: ANALYSIS REPORT

J. D. Shinn
J. Bean

New Mexico Engineering Research Institute
University of New Mexico
Albuquerque, NM 87131

August 1981

Final Report



Approved for public release; distribution unlimited.

THIS RESEARCH WAS SPONSORED BY THE DEFENSE NUCLEAR AGENCY UNDER SUBTASK H53BAXSX377, WORK UNIT 31, WORK UNIT TITLE: "STATISTICAL DATA ASSESSMENT."



AIR FORCE WEAPONS LABORATORY
Air Force Systems Command
Kirtland Air Force Base, NM 87117

AFWL-TR-80-152

This final report was prepared by the New Mexico Engineering Research Institute, University of New Mexico, Albuquerque, New Mexico, under Contract F29601-76-C-0015, Job Order WDMX0104 with the Air Force Weapons Laboratory, Kirtland Air Force Base, New Mexico. Mr. John N. Thomas (NTES) was the Laboratory Project Officer-in-Charge.

When Government drawings, specifications, or other data are used for any purpose other than in connection with a definitely Government-related procurement, the United States Government incurs no responsibility or any obligation whatsoever. The fact that the Government may have formulated or in any way supplied the said drawings, specifications, or other data, is not to be regarded by implication, or otherwise in any manner construed, as licensing the holder, or any other person or corporation; or as conveying any rights or permission to manufacture, use, or sell any patented invention that may in any way be related thereto.

This report has been authored by a contractor of the United States Government. Accordingly, the United States Government retains a nonexclusive, royalty-free license to publish or reproduce the material contained herein, or allow others to do so, for the United States Government purposes.

The Public Affairs Office has reviewed this report, and it is releasable to the National Technical Information Service, where it will be available to the general public, including foreign nationals.

If your address has changed, if you wish to be removed from our mailing list, or if your organization no longer employs the addressee, please notify AFWL/NTES, Kirtland AFB, NM 87117 to help us maintain a current mailing list.

This technical report has been reviewed and is approved for publication.

John N Thomas

JOHN N. THOMAS
Project Officer

FOR THE COMMANDER

James H. Lee Jr.

JAMES H. LEE, JR.
Lt Colonel, USAF
Chief, Technology & Applications Br

John C Galloway

JOHN C. GALLOWAY
Lt Colonel, USAF
Chief, Civil Engrg Research Div

---

DO NOT RETURN COPIES OF THIS REPORT UNLESS CONTRACTUAL OBLIGATIONS OR NOTICE ON A SPECIFIC DOCUMENT REQUIRES THAT IT BE RETURNED.

UNCLASSIFIED

SECURITY CLASSIFICATION OF THIS PAGE *(When Data Entered)*

| REPORT DOCUMENTATION PAGE | | READ INSTRUCTIONS BEFORE COMPLETING FORM |
|---|---|---|
| 1. REPORT NUMBER<br>AFWL-TR-80-152 | 2. GOVT ACCESSION NO.<br>AD-A108 | 3. RECIPIENT'S CATALOG NUMBER<br>268 |
| 4. TITLE *(and Subtitle)*<br>CYLINDRICAL IN SITU TESTS (CIST) 20 AND 21: ANALYSIS REPORT | | 5. TYPE OF REPORT & PERIOD COVERED<br>Final Report |
| | | 6. PERFORMING ORG. REPORT NUMBER<br>NMERI-DP/EM-34 |
| 7. AUTHOR(s)<br>J. D. Shinn<br>J. Bean | | 8. CONTRACT OR GRANT NUMBER(s)<br>F29601-76-C-0015 |
| 9. PERFORMING ORGANIZATION NAME AND ADDRESS<br>New Mexico Engineering Research Institute<br>University of New Mexico<br>Albuquerque, NM 87131 | | 10. PROGRAM ELEMENT, PROJECT, TASK AREA & WORK UNIT NUMBERS<br>62710H/WDMX0104 |
| 11. CONTROLLING OFFICE NAME AND ADDRESS<br>Air Force Weapons Laboratory (NTES)<br>Kirtland Air Force Base, NM 87117 | | 12. REPORT DATE<br>August 1981<br>13. NUMBER OF PAGES<br>50 |
| 14. MONITORING AGENCY NAME & ADDRESS*(if different from Controlling Office)*<br>Director<br>Defense Nuclear Agency<br>Washington, DC 20305 | | 15. SECURITY CLASS. *(of this report)*<br>Unclassified<br>15a. DECLASSIFICATION DOWNGRADING SCHEDULE |

16. DISTRIBUTION STATEMENT *(of this Report)*

Approved for public release; distribution unlimited.

17. DISTRIBUTION STATEMENT *(of the abstract entered in Block 20, if different from Report)*

18. SUPPLEMENTARY NOTES

This research was sponsored by the Defense Nuclear Agency under Subtask H53BAXSX377, Work Unit 31, Work Unit Title: "Statistical Data Assessment."

19. KEY WORDS *(Continue on reverse side if necessary and identify by block number)*

In Situ Testing
Material Modeling
Cylindrical In Situ Test (CIST)
Wave Propagation

20. ABSTRACT *(Continue on reverse side if necessary and identify by block number)*

The geologic in situ dynamic properties for near surface tuff and rhyolite were estimated based on measurements from CIST 21 and CIST 20, respectively. The resulting material models were expressed in terms of the AFWL Engineering Model.

DD FORM 1 JAN 73 1473

42171

UNCLASSIFIED

SECURITY CLASSIFICATION OF THIS PAGE *(When Data Entered)*

CONTENTS


| Section | | Page |
|---|---|---|
| I | INTRODUCTION | 5 |
| | Background | 5 |
| | Typical CIST Test | 6 |
| | CIST 20 and CIST 21 | 8 |
| II | CIST 21 ANALYSIS | 9 |
| | Test Site Description | 9 |
| | Instrumentation | 9 |
| | Data Analysis | 14 |
| | Pressure Boundary | 15 |
| | Material Model Development | 18 |
| III | CIST 20 ANALYSIS | 27 |
| | Test Site Description | 27 |
| | Data Analysis | 27 |
| | Pressure Boundary | 31 |
| | Material Model Development | 34 |
| IV | COMPARISON OF LABORATORY AND IN SITU MATERIAL PARAMETERS | 41 |
| V | CONCLUSIONS | 45 |
| | REFERENCES | 47 |


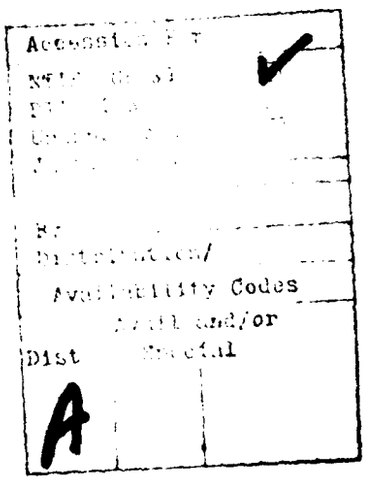

ILLUSTRATIONS


| Figure | | Page |
|---|---|---|
| 1 | Cross section of typical CIST site and instrumentation locations | 7 |
| 2 | Regional location of CIST events | 10 |
| 3 | Location map of CIST 21 within Hot Creek Canyon, Nevada | 11 |
| 4 | Cross section of hole and gage configuration with geological stratification, CIST 21 | 12 |
| 5 | CIST 21 core recovery | 13 |
| 6 | Time of arrivals versus range for CIST 21 | 16 |
| 7 | Peak radial velocity versus range | 17 |
| 8 | Comparison of CIST 21 pressure function to data | 19 |
| 9 | Initial properties for CIST 21 | 21 |
| 10 | Recommended properties for CIST 21 | 22 |
| 11 | Comparison of experimental and numerical radial velocity waveforms for CIST 21 at 0.91-m range | 23 |
| 12 | Comparison of experimental and numerical radial velocity waveforms for CIST 21 at 1.53-m range | 24 |
| 13 | Comparison of experimental and numerical radial velocity waveforms for CIST 21 at 2.44-m range | 25 |
| 14 | Comparison of experimental and numerical radial velocity waveforms for CIST 21 at 3.67-m range | 26 |
| 15 | Location of CIST 20 in Ralston Valley, Nevada | 28 |
| 16 | Cross section of hole and gage configuration with geological stratification, CIST 20 | 29 |
| 17 | Rock core from CIST 20 | 30 |
| 18 | CIST 20 time of arrival | 32 |
| 19 | CIST 20 peak particle velocity versus range | 33 |
| 20 | Comparison of experimental cavity pressure and functional fit used in calculations for CIST 20 at 6.42-m depth | 35 |
| 21 | Comparison of experimental cavity pressure and functional fit used in calculations for CIST 20 at 10.85-m depth | 36 |
| 22 | Recommended properties for CIST 20 | 37 |
| 23 | CIST 20: Comparison of experimental radial velocity waveforms and radial velocity waveforms from one-dimensional calculations for gages above water table | 39 |
| 24 | CIST 20: Comparison of experimental radial velocity waveforms and radial velocity waveforms from one-dimensional calculations for gages below water table | 40 |
| 25 | Loading P-V curves for Unit 3 tuff and Units 4a and 4b tuff | 43 |

TABLES


| Table | | Page |
|---|---|---|
| 1 | Ratio of peak vertical velocity to peak radial velocity | 15 |

# I. INTRODUCTION

## BACKGROUND

In recent years extensive theoretical and experimental research programs have been funded in an effort to quantify the response of strategic structures to airblast and ground shock loadings. The success of a soil- (or rock-) structure interaction analysis, whether static or dynamic, depends not only on the accurate simulation of the structure but also on the mathematical material models which are used to describe the behavior of the geologic materials which surround the structure. Thus a prime requirement for predicting the response of strategic structures to nuclear and high explosive blast loadings is an understanding of the response of geologic materials to high intensity impulsive loads.

There are several advanced constitutive models that may be used in ground shock computer codes. Among the more popular are the Weidlinger Associates Cap Model (Ref. 1) and the Air Force Weapons Laboratory (AFWL) Engineering Model (Ref. 2). Some newly developed constitutive models include Lade's Model (Ref. 3), Prevost's Model (Ref. 4), and the Systems, Science and Software Endochronic Model (Ref. 5). A summary of some of the important features of each of these models is included in Reference 6.

Until recently the data required to evaluate the parameters in the various models were obtained from laboratory tests performed on undisturbed specimens. The tests included uniaxial strain and triaxial shear. Unfortunately there exist large discrepancies between computer code predictions using laboratory-derived material models and experimental field measurements. It is generally agreed that major contributors to these differences are sample disturbance and the inability to properly characterize a site by testing a limited number of soil or rock samples.

To avoid the difficulties associated with laboratory testing, in situ tests have been developed and are becoming increasingly popular in the geotechnical community. One such test, the Cylindrical In Situ Test (CIST), was developed by AFWL to aid in the determination of the in situ dynamic properties of the geologic material. Thus laboratory testing may be supplemented with in situ measurements and from this synthesis of information the appropriate material parameters can be determined.

## TYPICAL CIST TEST

Figure 1 (Ref. 7) illustrates the major features of a typical CIST experiment. The CIST consists of a vertical cylindrical cavity 0.61 m in diameter drilled to a depth several meters below the deepest gage location. The explosive source placed within the cavity consists of 400-gr PETN (pentaerythritol tetranitrate) detonating cord wrapped on racks to give a uniform loading density of approximately 1.5 kg/linear meter. The explosive configuration is designed to generate a peak pressure at the cavity wall of approximately 41.4 to 48.3 MPa upon detonation. The vertical cylindrical loading geometry offers the obvious advantage that near surface horizontal layers can be exercised with a minimum of interactions among layers.

Accelerometers are a primary source of ground motion data obtained from a CIST. Radial sensing accelerometers are typically placed at ranges of 0.91 m, 1.52 m, and 2.44 m from the centerline of the CIST cavity. Vertically sensing accelerometers are sometimes placed at these locations to provide an estimate of the one-dimensional simulation time beyond which two-dimensional effects become important. Other instrumentation used in CIST includes cavity pressure and soil stress gages.

Cavity pressure gages are placed in contact with the cavity wall and the data recorded can provide an estimate of the pressure/time history resulting from the detonation of the explosive array. The experimental cavity pressure records are sometimes represented analytically by a decaying exponential relation. In this form it may be used as input for the finite difference code in the development of the material models for the site.

Material models are developed by systematically and logically varying the parameters which describe the assumed mathematical form of the model until a combination results in a reasonable approximation to the experimental data. In CIST analysis the radial velocity/time histories, obtained by integrating the radial accelerometer records, are compared with the computer-generated radial velocity/time histories.

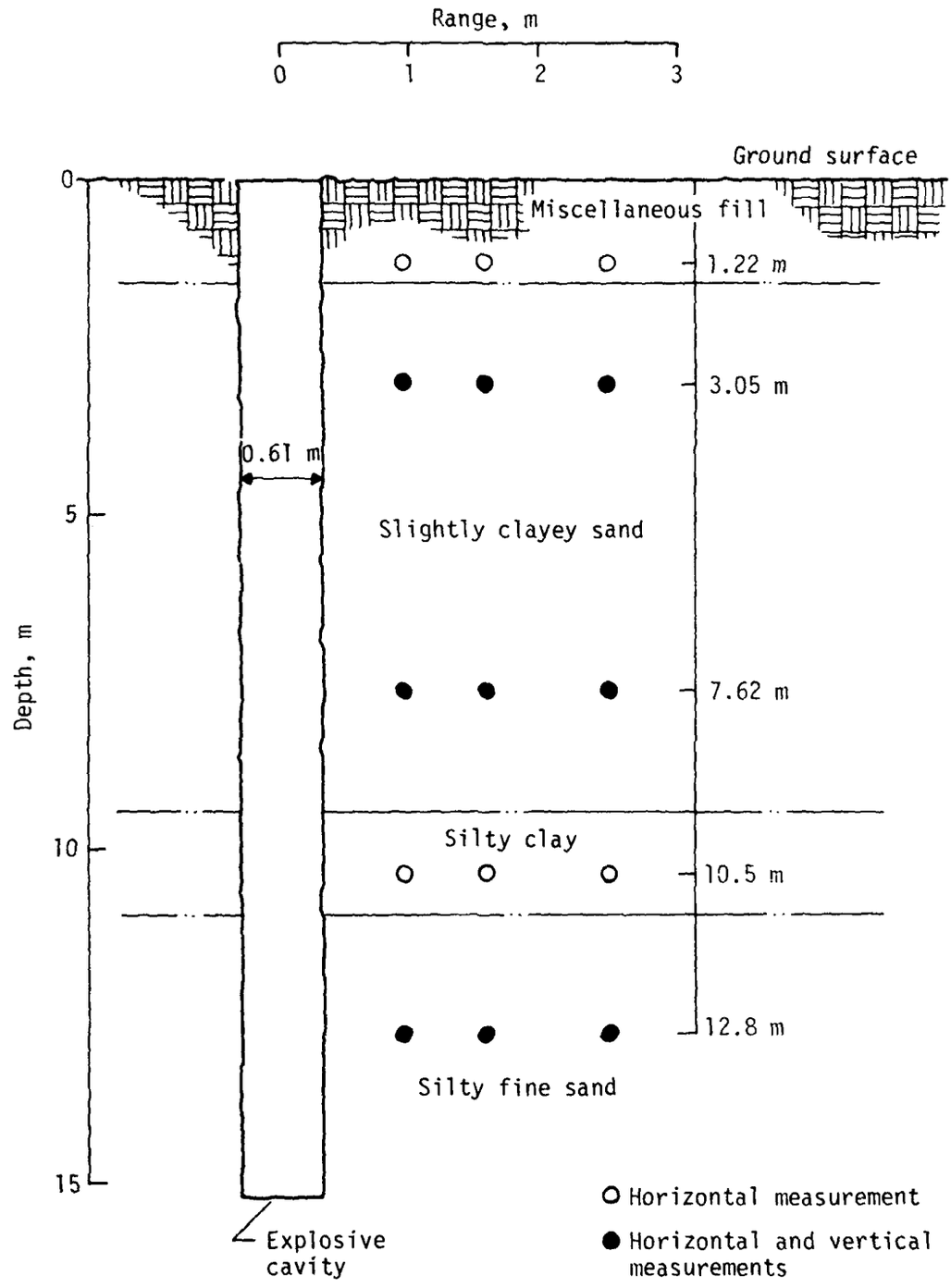


Figure 1. Cross section of typical CIST site and instrumentation locations (Ref. ).

CIST 20 and CIST 21

One general class of geologic material that may be encountered in the proposed Missile-X (MX) siting areas are those of volcanic origin. In an effort to obtain representative dynamic material properties for the Nevada volcanic rocks, CIST 20 was conducted in rhyolite at Ralston Valley, Nevada and CIST 21 was conducted at Hot Creek Canyon, Nevada in tuff. Previous CIST experiments have been performed in alluvium and playas.

The objective of this analysis report is to present material models developed for tuff and rhyolite rocks. The analysis of CIST 21 (Section II) is presented first because the experimental data were of higher quality, which resulted in a more detailed analysis. The analysis of CIST 20, presented in Section III, was limited in scope as the data quality did not warrant extensive investigation. Section IV presents a comparison of laboratory and in situ material parameters obtained from tests performed on Nevada Test Site (NTS) tuff. Section V summarizes the results and provides suggestions for improving testing in rock materials.

## II. CIST 21 ANALYSIS

### TEST SITE DESCRIPTION

CIST 21 was conducted in Hot Creek Canyon, east of Warm Springs, Nevada (Figs. 2 and 3). The geologic profile (Fig. 4) shows that the site consisted of moderately welded tuff overlain by a thin surface layer of silty sand. The water table was located 7.62 m below the ground surface. The in situ unit weight of the tuff can vary between 2160 and 2350 kg/m$^3$ depending upon the degree of saturation. Laboratory tests indicated that the tuff at the test site had a dry density of 2157 kg/m$^3$, a specific gravity of 2.671, and a void ratio (volume of voids divided by volume of solids) of 0.232. Figure 5, a photograph of rock core obtained from the site, suggests that the tuff was relatively free of jointing. The Rock Quality Designation index (RQD) was not calculated at the time of drilling. Because some of the core was missing at the time of this analysis, RQD could not be determined.

### INSTRUMENTATION

Ground motion data were obtained from accelerometers located at four depths (3.96 m, 5.18 m, 9.14 m, and 12.19 m). At each depth, four ranges (0.91 m, 1.52 m, 2.44 m, and 3.66 m) were instrumented. (Based upon borehole inclinometer surveys of instrumentation holes in CIST 23, radial position errors can be as great as plus or minus 150 mm.) Radial and vertically sensing accelerometers were located at the 3.96- and the 12.19-m depths, while only radial accelerometers were used at the two intermediate depths. In addition to the accelerometers fielded, cavity pressure measurements were made at the 3.96-, 5.18-, and the 9.14-m depths. Thus two depths above and two depths below the water table were instrumented. No soil stress gages were used in CIST 21.

In general the quality of the data was adequate; however, a large percentage ($\simeq$ 70 percent) of the data records had early time failures. Those measurements which did last for periods of time exceeding 20 ms had baseline offsets. The instrumentation failures caused difficulties in the data analysis because the unload portion of the motion pulse could not be accurately modeled. This resulted in uncertainties in material model development because the unload portion of the velocity pulse was influenced by the yield surface used in the material model (AFWL Engineering Model).

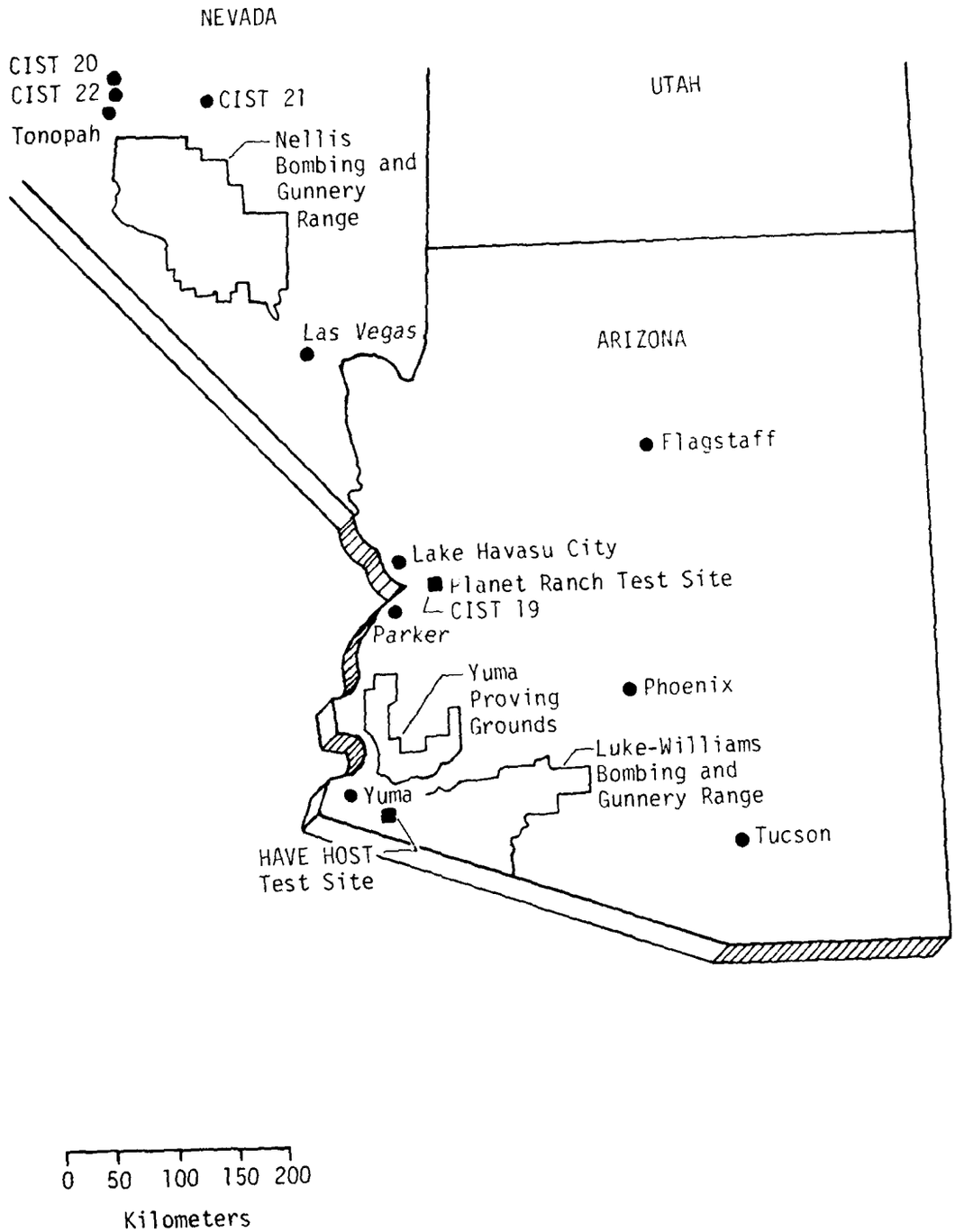


Figure 2. Regional location of CIST events.

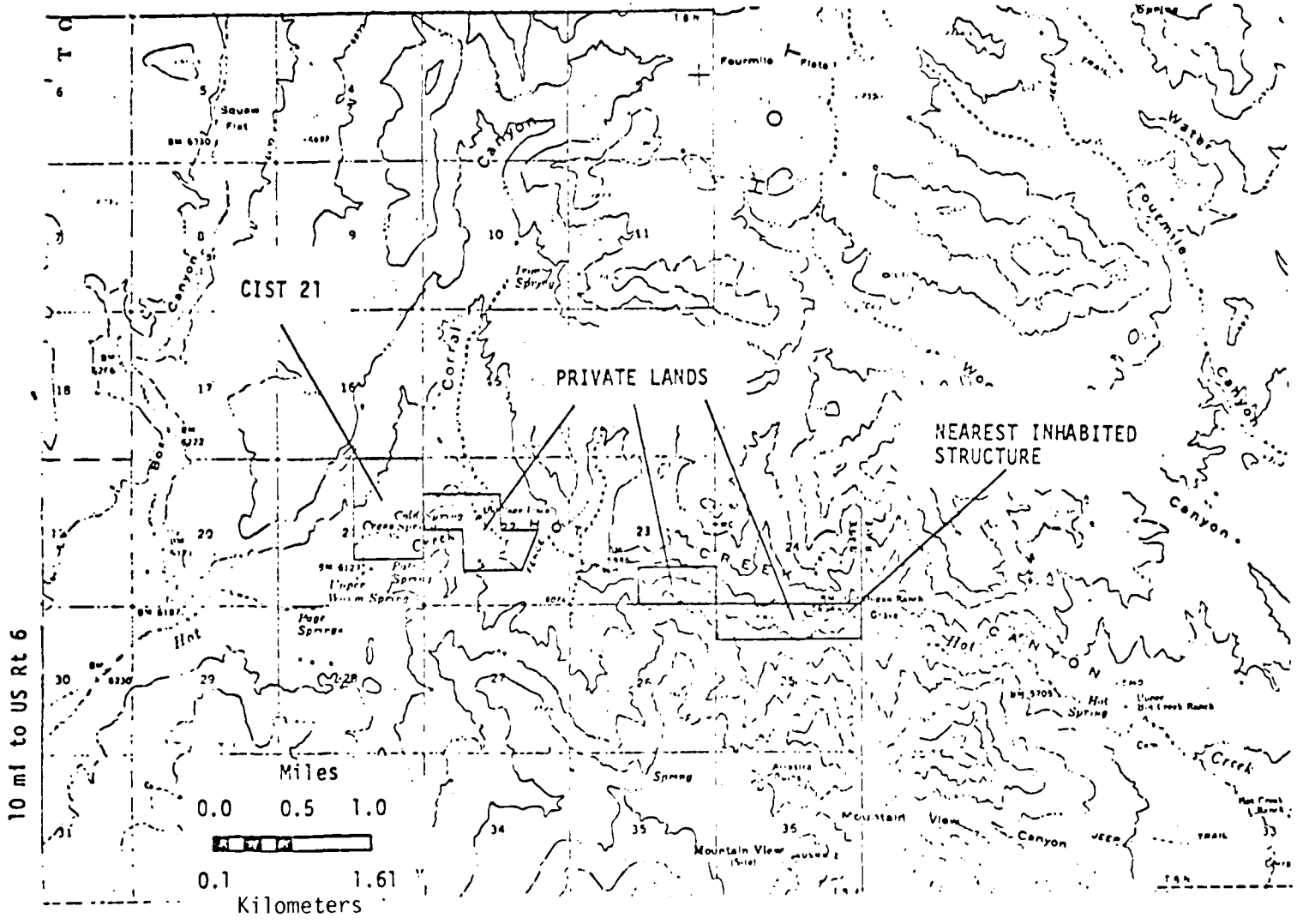


Figure 3. Location map of CIST 21 within Hot Creek Canyon, Nevada.

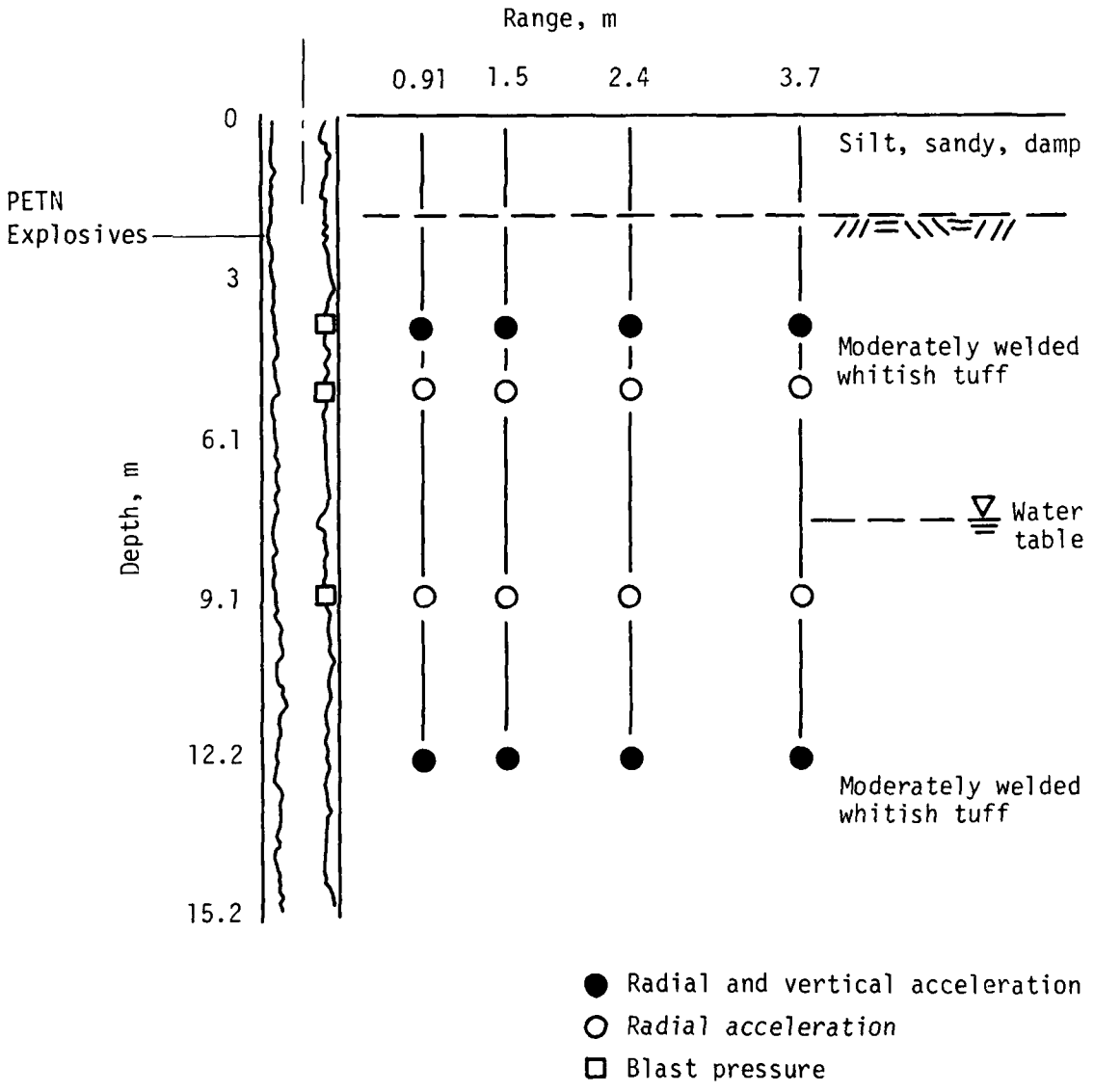


Figure 4. Cross section of hole and gage configuration with geological stratification, CIST 21.

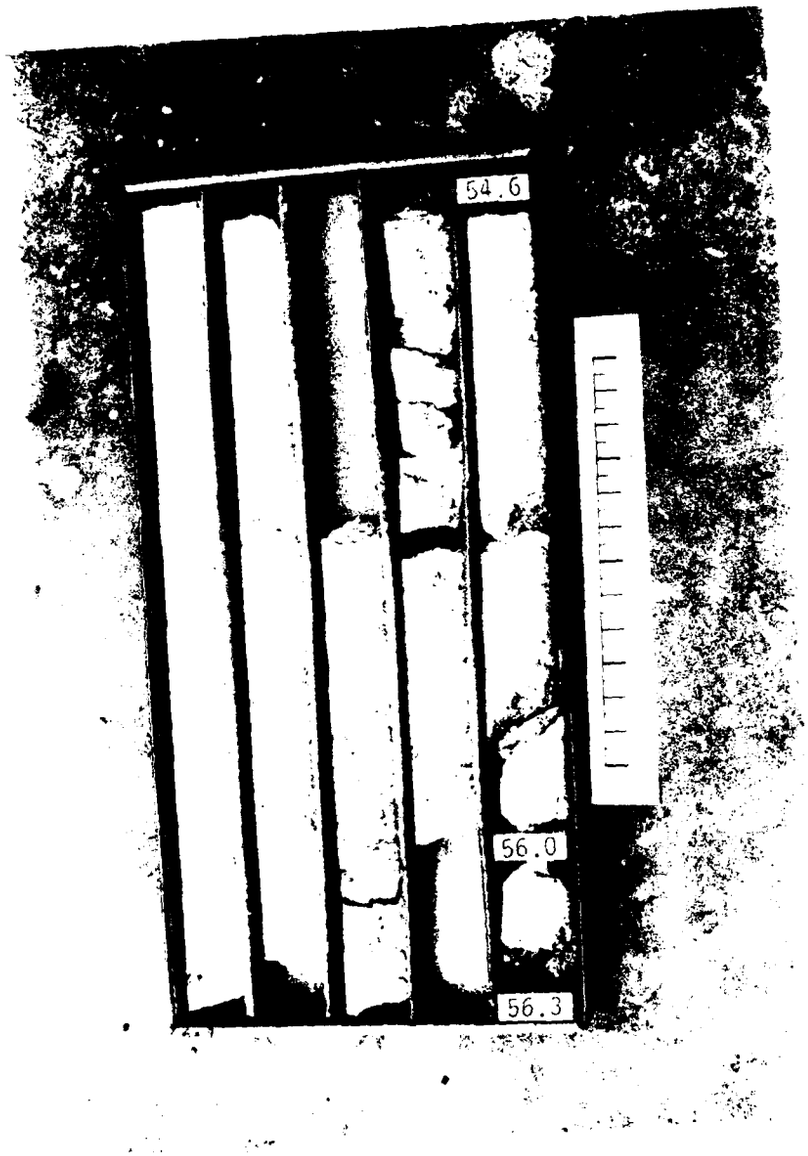


Figure 5. CIST 21 core recovery.

## DATA ANALYSIS

The analysis of CIST 21 consisted of examining the experimental waveforms (integrated accelerometer records, i.e., particle velocity) to aid in determining some of the initial estimate material model parameters. Using the initial parameters a one-dimensional finite difference calculation was performed in an attempt to match the experimental records. Comparing the experimental and numerical waveforms, the model parameters were updated in an attempt to better match the experimental data. The iterative procedure was performed using the CERF Soil Parameter Iterative Code (SPI) (Ref. 8). Basically the SPI code is a nonlinear curve fitter coupled to a one-dimensional wave propagation code (WONDY, Ref. 9) which seeks the set of material property parameters that results in the best fit of the experimental radial velocity/time histories.

In utilizing a one-dimensional code to evaluate CIST events the magnitude and time of arrival of two-dimensional effects in the radial waveforms must be estimated. Theoretically the occurrence of any vertical motion is an indication of multidimensional effects which may be caused by the finite length of the CIST cavity and the free surface. Such effects may be deduced by comparing experimental radial and vertical velocity waveforms at the same gage locations. In CIST 21 the middle two gage depths did not have vertically sensing gages; therefore the arrival of two-dimensional effects had to be estimated from the other gage locations.

Future CIST events should have vertical motion measurements at all radial motion measurement locations. These gages are necessary for determining two-dimensional effects and also for comparison with two-dimensional calculations. It should be noted that one-dimensional calculations are not necessarily adequate for CIST analysis but should be viewed as preliminary to two-dimensional analysis.

CIST 21 appeared to have more early time two-dimensional effects than normally observed in CIST events. This conclusion was based on the empirical rule which assumes that if the ratio of vertical to radial velocity is 0.1 or less, the test may be considered predominantly one-dimensional. Table 1 summarizes the vertical to horizontal velocity ratio calculated at the 3.96- and 12.19-m depths. The 12.19-m depth data do not fit the assumption of one-dimensionality, and the 3.96-m depth also has larger vertical motions than are desirable. After carefully examining the experimental waveforms, the

decision was made to treat the experiment as one-dimensional for the first 10 to 15 ms. Two-dimensional effects are believed to control the motions at later times and can only be examined by the use of two-dimensional codes.

TABLE 1. RATIO OF PEAK VERTICAL VELOCITY TO PEAK RADIAL VELOCITY

| Depth, m | Range, m | | | |
|---|---|---|---|---|
| | 0.91 | 1.52 | 2.44 | 3.66 |
| 3.96 | 0.33 | 0.14 | 0.07 | 0.28 |
| 12.19 | 0.40 | No data | 0.45 | 0.33 |

Plots for time of first arrival versus range and time of arrival of the peak radial particle velocity versus range are shown in Figure 6. There appears to be little variation with depth in the seismic wave speed, $C_i$, and the velocity of the plastic wave, $C_p$. Therefore the material properties of the tuff above and below the water table were indistinguishable on the basis of wave speeds observed. This may also be inferred from Figure 7 where peak radial particle velocity versus range for all gage depths is plotted. The variation in peak particle velocity at each range shows little variation with depth except for the far range at the 12.19-m depth. As was shown earlier, this depth was highly two-dimensional and it is not surprising that the peak velocities attenuated differently from the other gage depths. The CIST 21 peak radial particle velocities attenuated at approximately $R^{-1}$. By comparison elastic theory predicts cylindrically expanding waves attenuate at $R^{-1/2}$.

## PRESSURE BOUNDARY

A pressure boundary was used to drive the calculation in the CIST 21 analysis. This was done by fitting a function of the form

$$P(t) = P_o \left(1 - \frac{t}{t_o}\right)^N \qquad (1)$$

where

$P(t)$ = pressure in megapascals

$P_o$ = peak pressure in megapascals

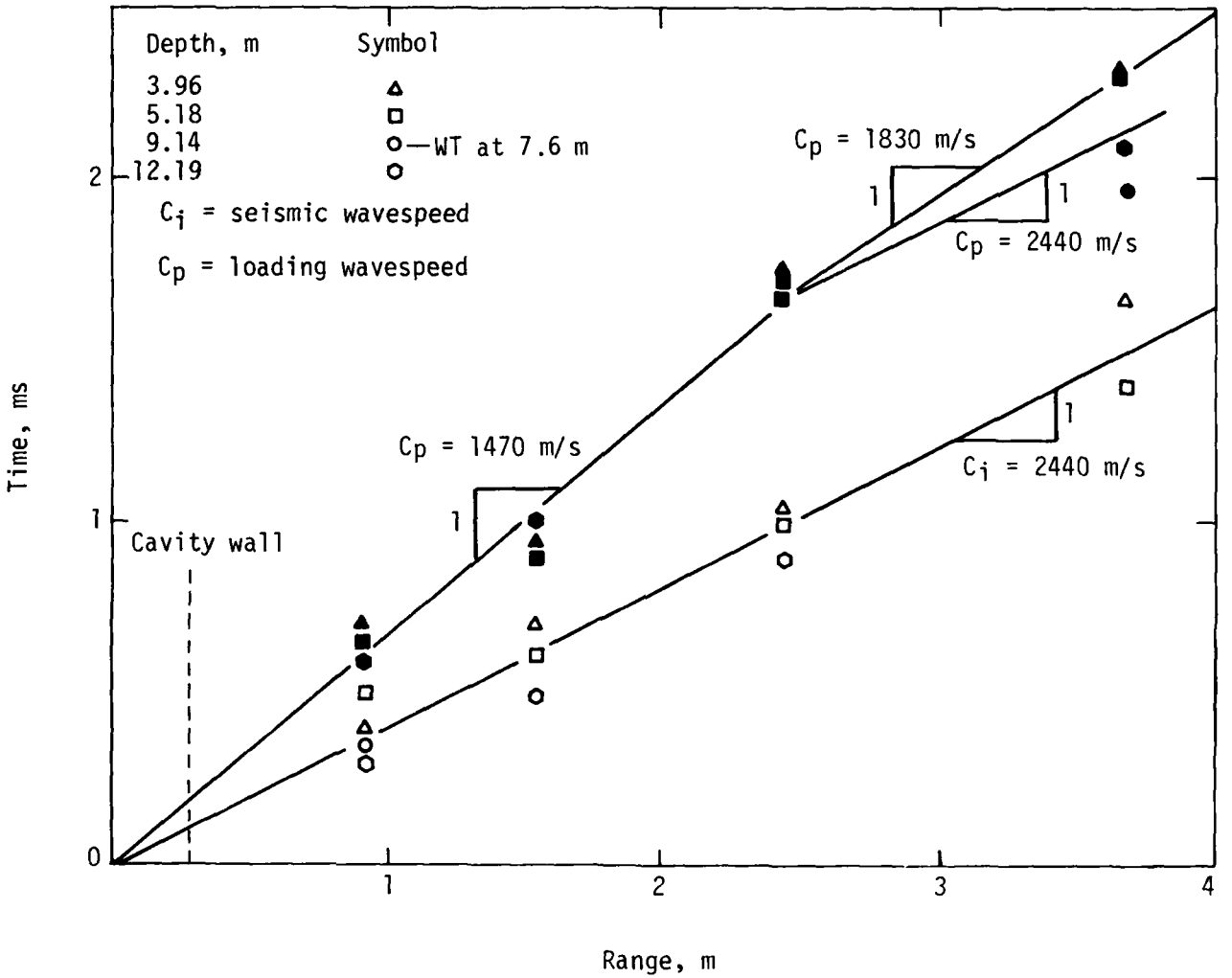


Figure 6. Time of arrivals versus range for CIST 21.

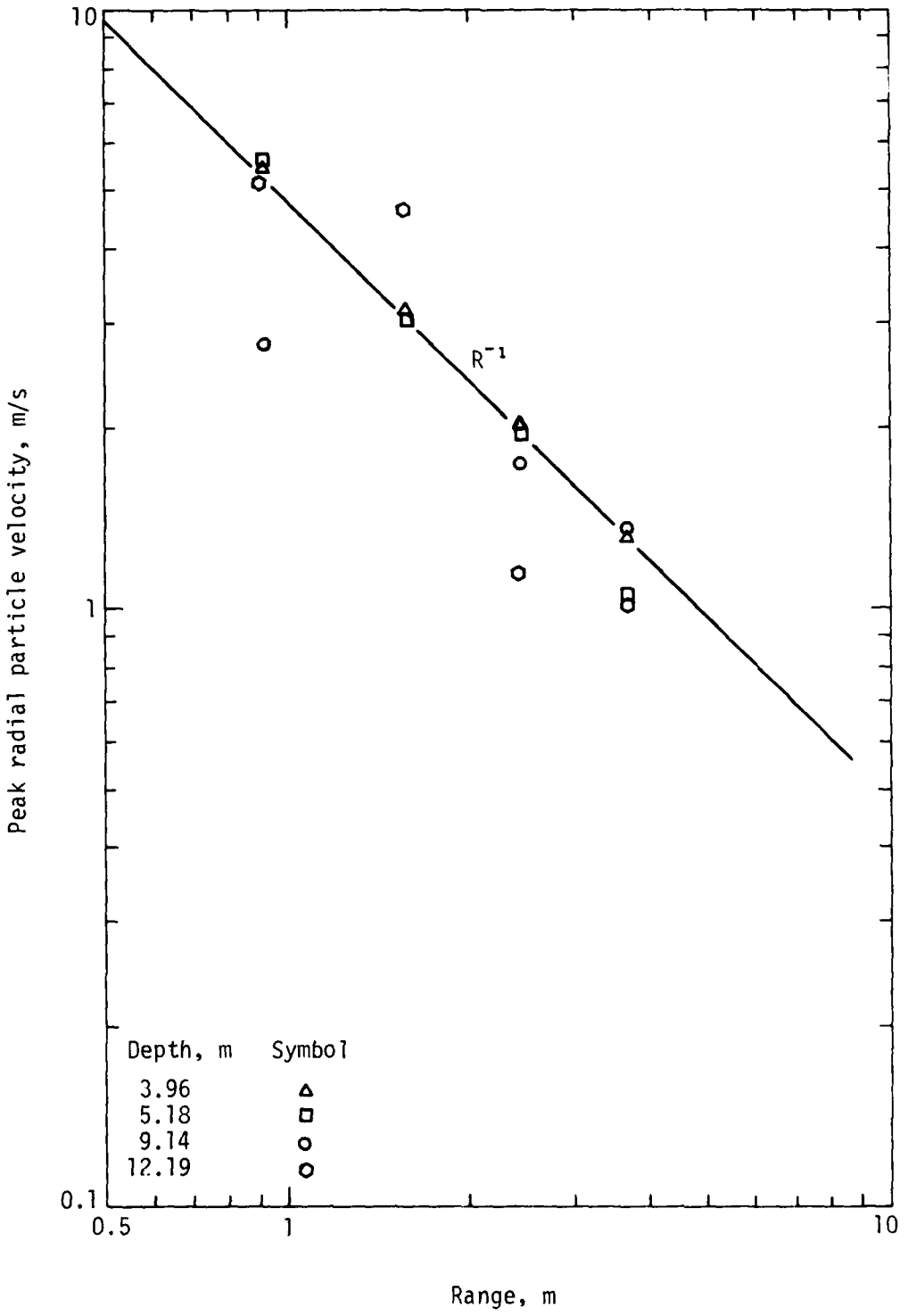


Figure 7. Peak radial velocity versus range.

$t_o$ = total duration of the positive phase in milliseconds

$t$ = time in milliseconds

$N$ = decay constant

to cavity pressure measurements. Unfortunately only one reliable measurement was available and it malfunctioned after 12 ms. Figure 8 shows the experimental cavity pressure record and the curve that was chosen to fit it. The resulting equation used in the analysis was

$$P(t) = 34.5 \text{ MPa} \left(1 - \frac{t}{100}\right)^{10} = 5000 \text{ lb/in}^2 \left(1 - \frac{t}{100}\right)^{10} \qquad (2)$$

There are two major differences in the experimental data and the curve fit which will affect the calculational modeling.

1. The oscillatory nature of the experimental data is not reflected in the function presented above; however, it is believed that the tuff is capable of transmitting these oscillations. Comparing the experimental motion data to the calculated waveforms, the oscillatory nature of the measurements will not be seen in the calculated data. This difference was assumed to be insignificant.

2. Because there were no data records at late time the venting of the CIST cavity could not be modeled. There are some empirical rules for modeling late time cavity venting as a function of depth of the cavity. Because venting occurs first at the surface and proceeds down the length of the cavity, the decay functions result in more impulse at the bottom of the cavity. There appears to be so much uncertainty in these empirical rules that varying the decay as a function of depth was not considered justifiable. The pressure function was thus assumed to be representative for the entire cavity.

## MATERIAL MODEL DEVELOPMENT

The first time of arrival plots and the time of arrival of the peak radial velocity plots in Figure 6 were used to estimate the uniaxial wave speeds and moduli for the tuff at the CIST 21 test site. The break points in the uniaxial model were estimated by calculating a stress utilizing the peak velocity. Examination of Figure 6 indicates that between the 2.44- and 3.66-m ranges the plastic wave velocity, $C_p$, appeared to be approaching the elastic wave velocity, $C_i$. This suggests that the tuff was becoming elastic. This trend was also observed in the experimental waveforms as the rise time to peak became less

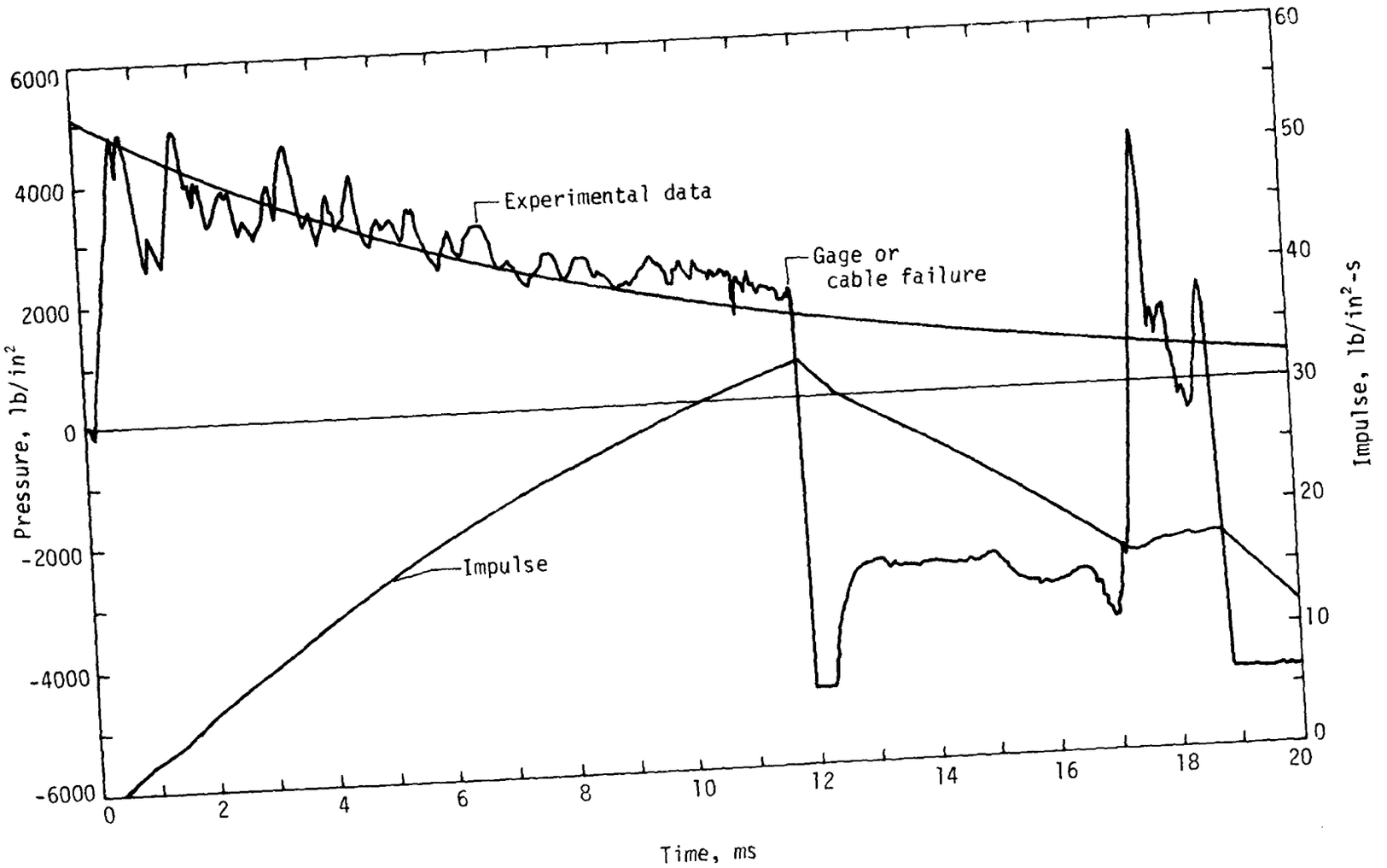


Figure 8. Comparison of CIST 21 pressure function to data.

past the 2.44-m range. Utilizing the peak particle velocity at the 3.66-m range, the elastic toe of the uniaxial model was then estimated to occur at 4.14 MPa (600 lb/in$^2$). A weak rock failure surface was used as the initial estimate in the code calculation. The initial material model parameters utilized in evaluating CIST 21 are shown in Figure 9.

Because the experimental data at the 3.96-m depth was judged to be the highest quality, calculations were first carried out by attempting to reproduce numerically the radial velocity/time histories at that depth. Calculations for the 5.18- and the 9.14-m depths resulted in material models that were similar to those derived for the 3.96-m depth. The recommended material properties for tuff are shown in Figure 10. A comparison of the experimental and numerically generated waveforms for the initial and recommended material model is shown in Figures 11 through 14. The calculations do not match all of the features of the experimental data, especially the late time decay rate. This was believed to be partly due to the occurrence of two-dimensional effects and the overall quality of the data. The rapid attenuation past the peak in the data could not be matched by the calculation using the properties given in Figure 10. In an effort to determine if a different set of parameters would result in a better match to the experimental data, another set of calculations was performed. Because the hydrostatic relation was judged to be representative of the experimental data, only the parameters related to the failure surface were varied. The variations included 1) increasing the Von Mises limit, 2) increasing the intercept on the $\sqrt{J_2}$ axis (cohesion), 3) reducing the slope of the Drucker-Prager portion, and 4) increasing Poisson's ratio. None of the variations resulted in a better fit to the data, and the waveform changes observed were similar to those observed by Bratton and Higgins (Ref. 7). The material parameters recommended for tuff at the CIST 21 site shown in Figure 10 may be used to evaluate the response of near-surface tuffs at similar sites. Minor variations in either the failure surface or hydrostat will not significantly alter the calculated response of the media. However, if laboratory-derived material models are used, there may be significant errors due to the difficulties inherent to laboratory testing. This is discussed in Section IV of this report.

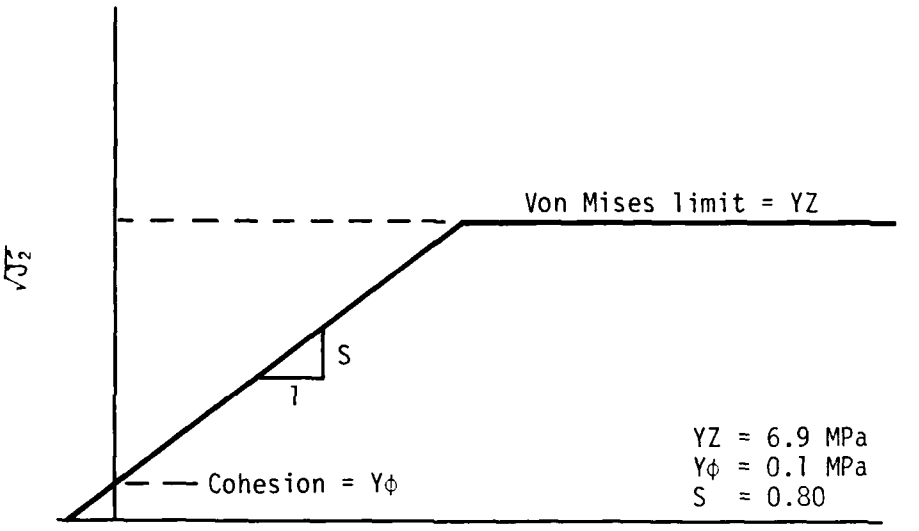


Yield surface

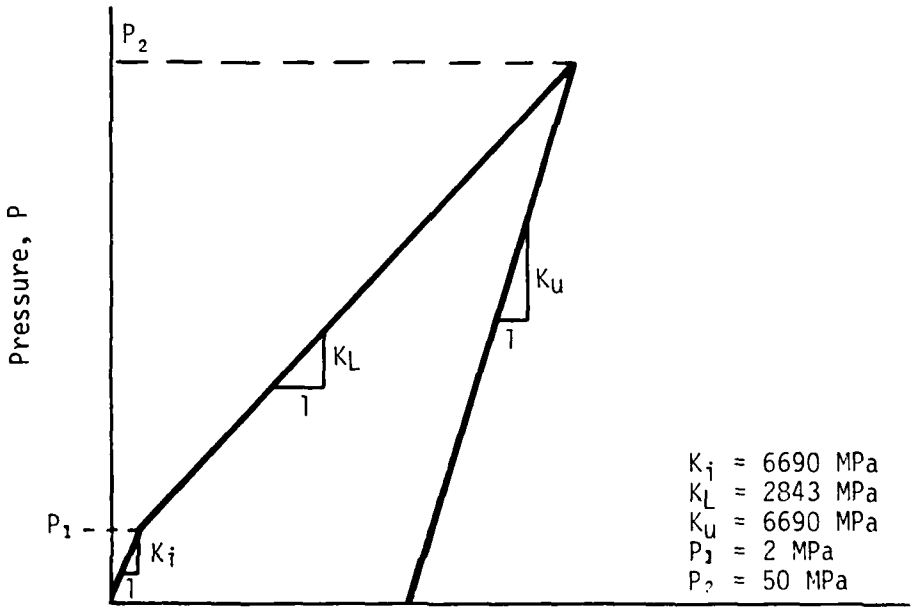


Hydrostat

Figure 9. Initial properties for CIST 21.

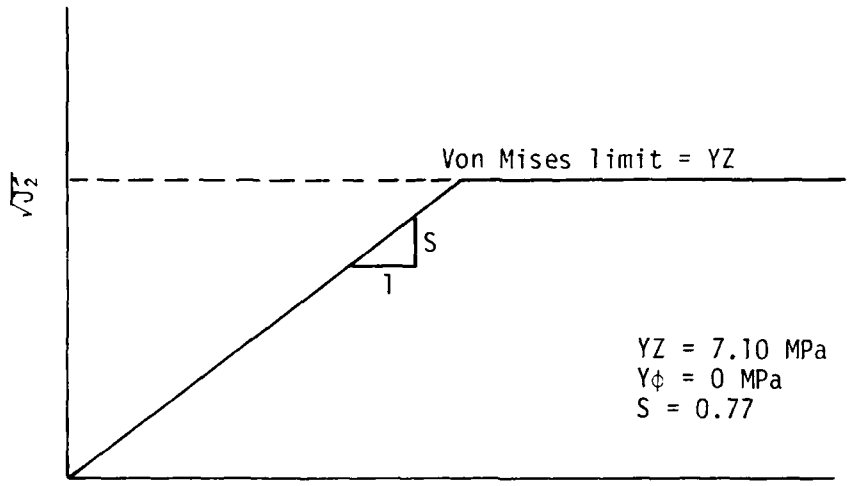


Pressure, p

Yield surface

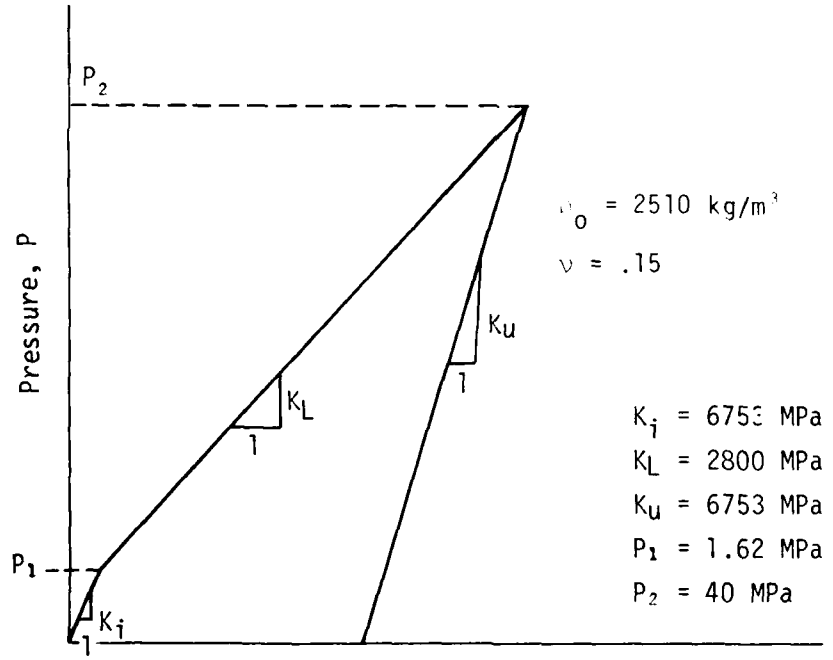


Excess compression, $\mu = \frac{\rho - \rho_o}{\rho_o}$

Hydrostat

Figure 10. Recommended properties for CIST 21.

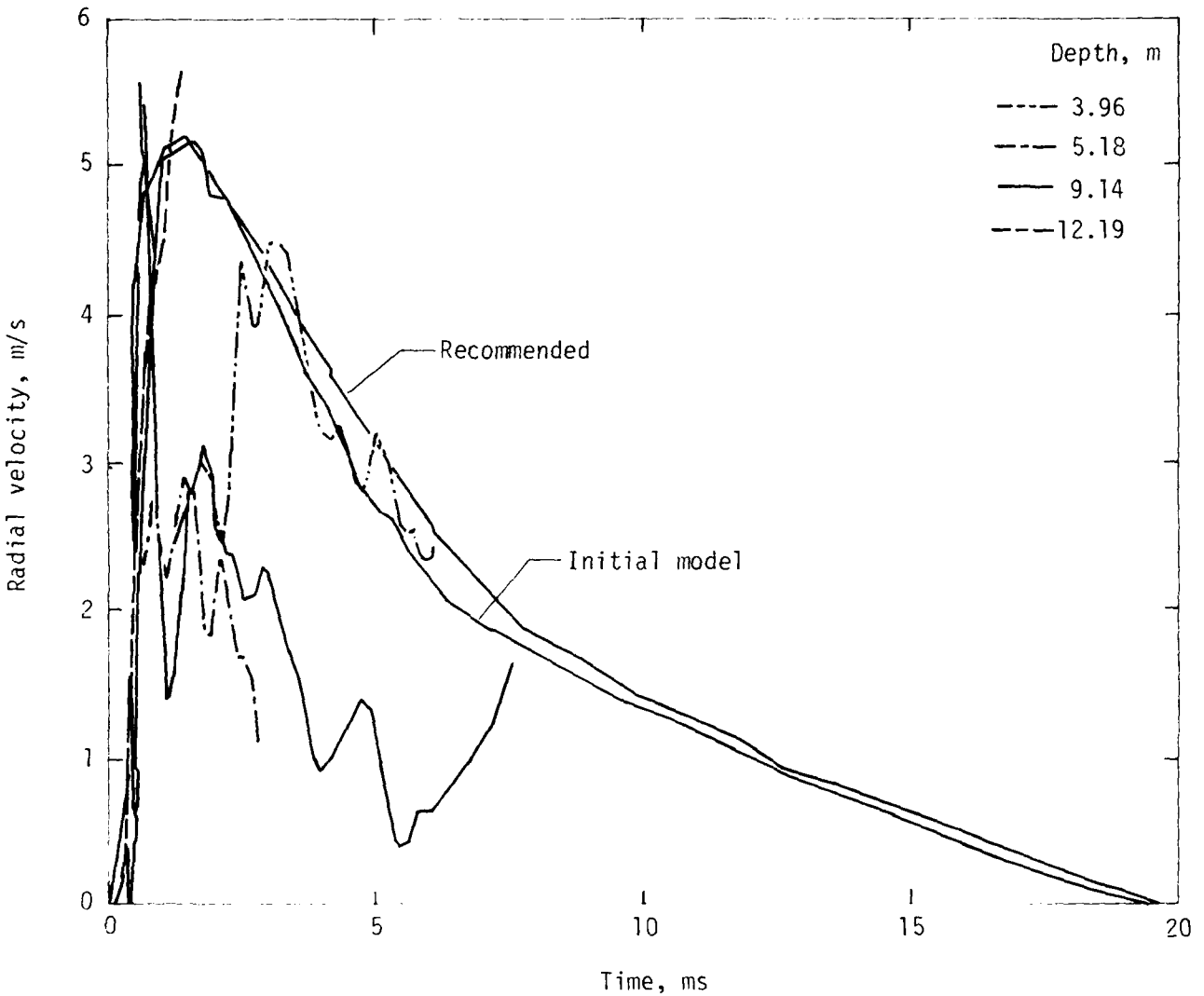


Figure 11. Comparison of experimental and numerical radial velocity waveforms for CIST 21 at 0.91-m range.

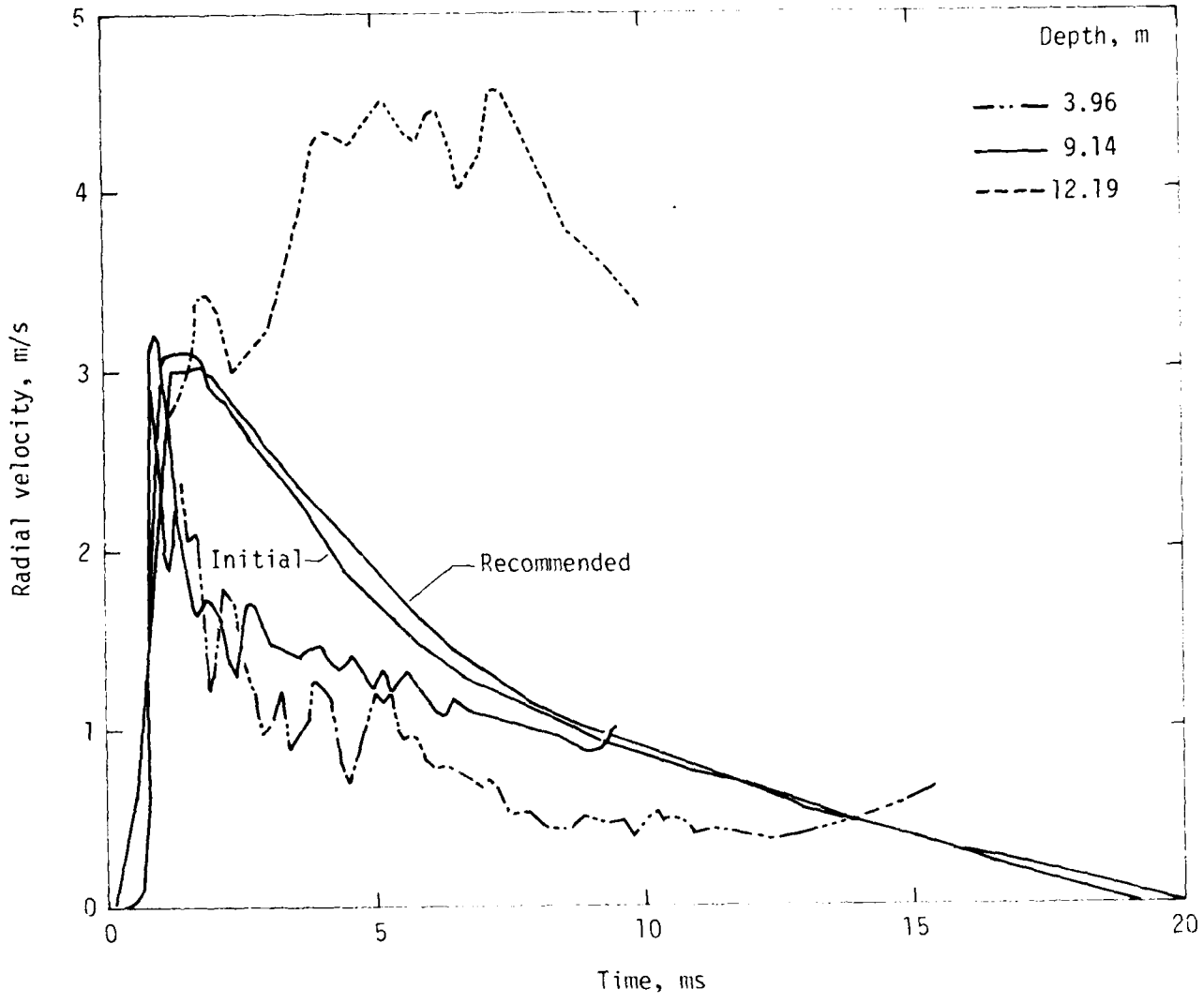


Figure 12. Comparison of experimental and numerical radial velocity waveforms for CIST 21 at 1.53-m range.

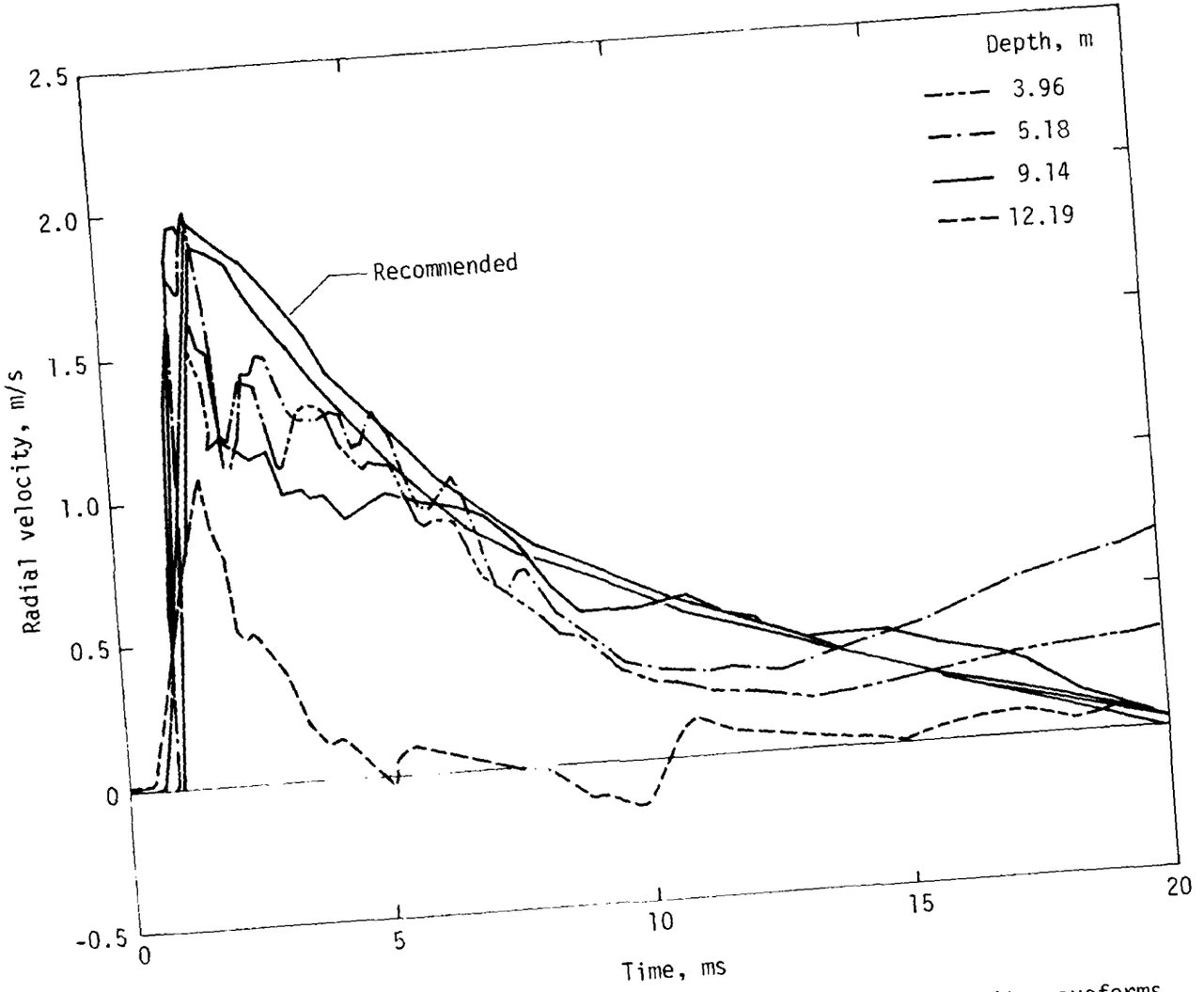


Figure 13. Comparison of experimental and numerical radial velocity waveforms for CIST 21 at 2.44-m range.

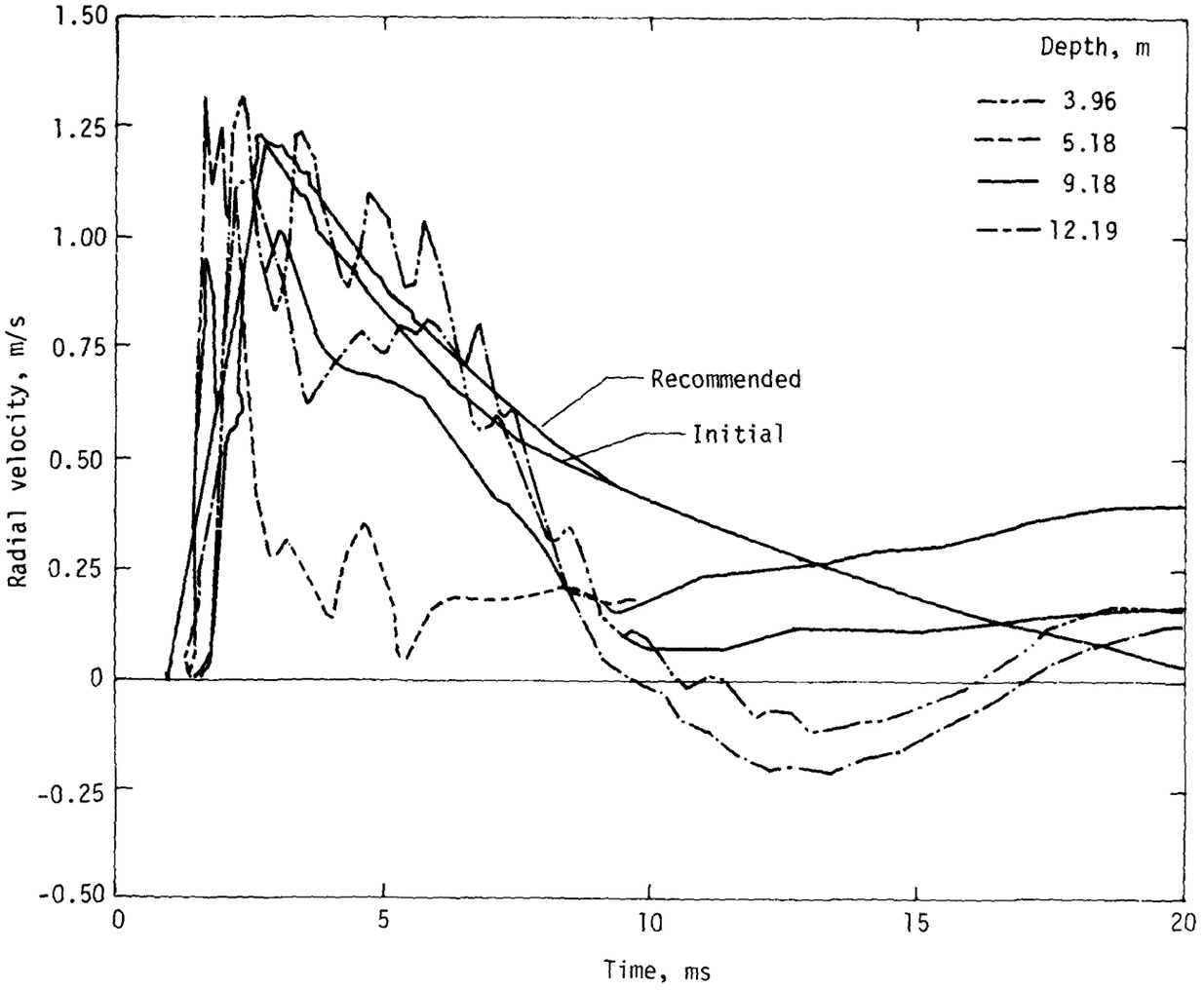


Figure 14. Comparison of experimental and numerical radial velocity waveforms *for* CIST 21 at 3.67-*m range*.

# III. CIST 20 ANALYSIS

## TEST SITE DESCRIPTION

CIST 20 was conducted at Ralston Valley [26 km, 30°N of Tonapah, Nevada on Bureau of Land Management land (Fig. 15)] on 29 August 1977. The site consisted of dry, dense rhyolite to a depth of 9.1 m below which the rhyolite was saturated (Fig. 16). Laboratory testing of rhyolite from the site showed the material to have a dry density of 2274 kg/m$^3$, a void ratio of 0.202, and a specific gravity of 2.74. Rock core obtained indicated that the rhyolite was highly jointed (Fig. 17). The jointing had a dramatic effect on the derived material model parameters when compared to the results of CIST 21. RQD was not determined during drilling operations.

Ground motion data were obtained at four depths (3.35 m, 6.4 m, 10.82 m, and 13.72 m); at each depth four ranges were instrumented (0.91 m, 1.52 m, 2.44 m, and 3.66 m). Thus two depths above and two depths below the water table were instrumented. Cavity pressure measurements were obtained at three positions.

In general the data recovery for CIST 20 was considered poor. Only 30 percent of the gages survived longer than 30 ms and only 15 percent survived longer than 100 ms. This makes correcting the data very difficult. In addition nearly all the channels had noise bursts which obscured the data, thus making the analysis very difficult. Before additional CISTs are fielded in rock materials, new protection schemes should be devised to ensure adequate data recovery. The behavior of fractured rock can be very complicated and these complications make detailed analysis impossible without high quality data.

## DATA ANALYSIS

The analysis of CIST 20 was similar to that for CIST 21. Initial material properties were estimated from the experimental data. Wave speeds and breakpoints (changes in hydrostat slopes) were estimated from time of arrival (first arrival and arrival of peak) and the peak radial particle velocity plots. Unlike the CIST 21 data, which showed little scatter with depth, the CIST 20 data varied greatly in both arrival times and attenuation rates.

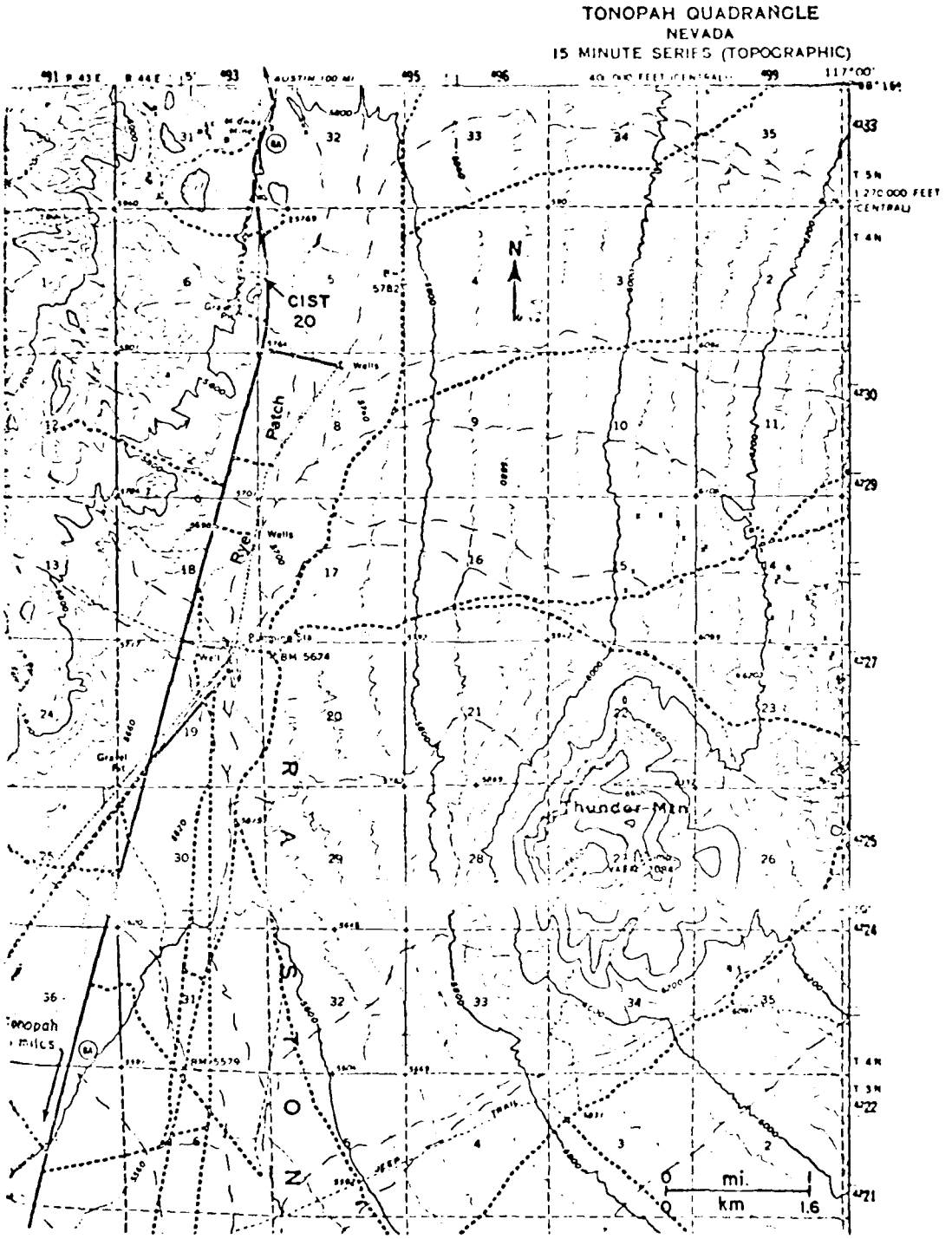


Figure 15. Location of CIST 20 in Ralston Valley, Nevada.

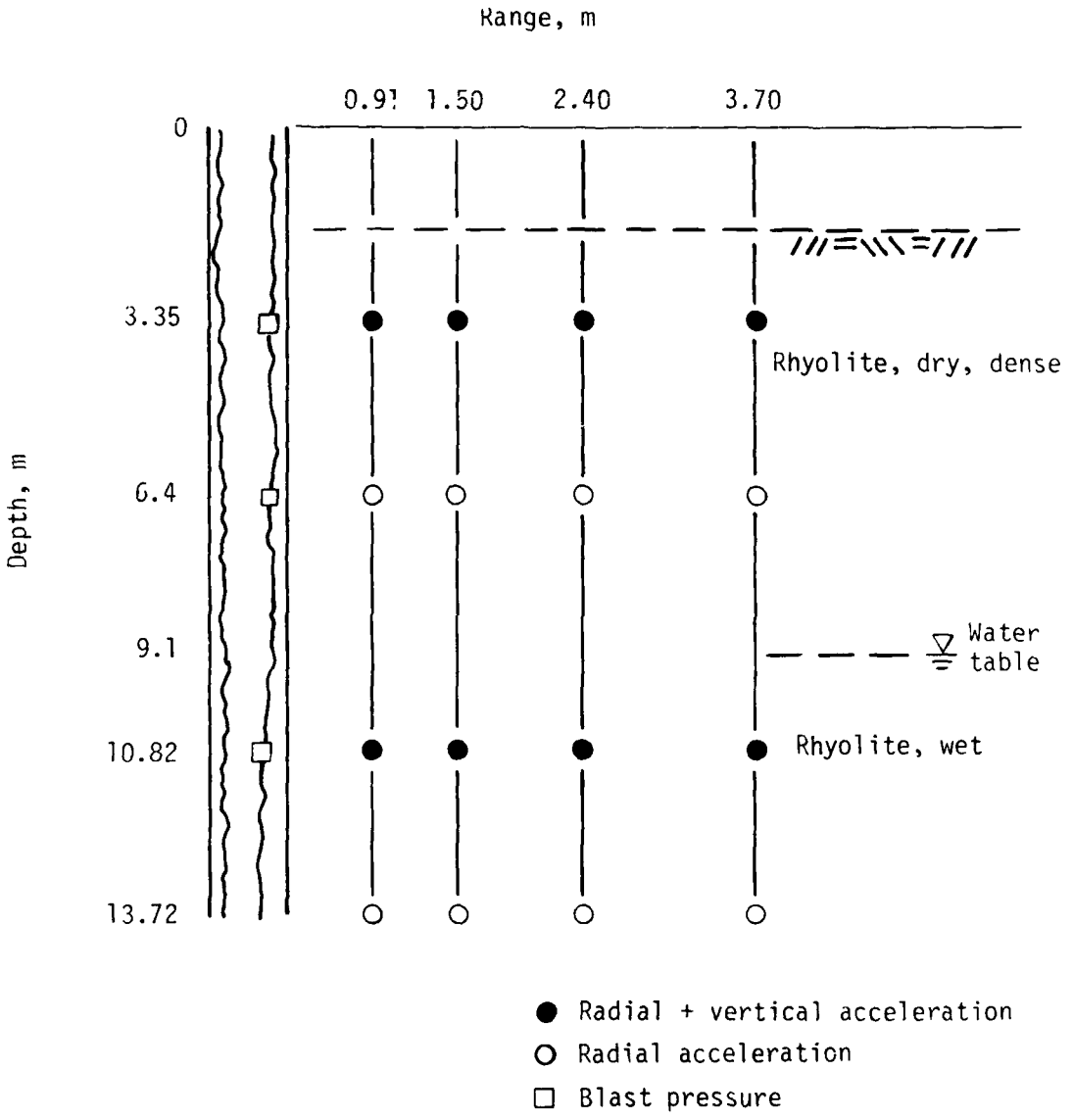


Figure 16. Cross section of hole and gage configuration with geological stratification, CIST 20.


Figure 17. Rock core from CIST 20.

The first time of arrival plots, shown in Figure 18, indicate that the rhyolite above the water table has an initial seismic wave speed of 1800 m/s. Below the water table the seismic wave speed is significantly higher at 3200 m/s.

Thus, while the tuff at CIST 21 did not show any apparent differences because of the influence of the water table, the same is not true for the rhyolite tested at CIST 20. Time of arrival of the peak particle velocity is not shown due to data quality and scatter.

The peak particle velocity versus range plot is shown in Figure 19. As can be seen, the data has a great deal of scatter. None of the close-in measurements survived longer than 2 ms. Thus the symbols with the "+" sign indicate that the gage may have malfunctioned prior to the arrival of the peak. A comparison of peak particle velocities indicates that, in general, CIST 20 particle velocities were higher than those from CIST 21. This indicates that the rhyolite is more compressible than the tuff at CIST 21, provided the loading functions were equal.

The particle velocities at the 0.9-m range (Fig. 19) were judged to be less than the peak because larger velocities were recorded at the 1.5- and the 2.4-m ranges. Therefore less importance was placed on the data from the 0.9-m range for CIST 20 analysis. The data from the 2.4- and 3.65-m ranges were given the most consideration because the data appeared to be more reliable and consistent. In addition the measurements made above the water table were analyzed in greater detail than those below because the data quality was better. Below the water table the record at the 10.82-m depth and 2.4-m range was considered to be the only usable information in terms of one-dimensional analysis. In the CIST 21 analysis it was shown that the deepest gage location was highly two-dimensional. This was assumed to also be true for CIST 20. The assumption seems valid since the particle velocities at the 13.72-m depth are much less than those measured at the shallower depths. Because no vertically sensing gages were placed at 13.72 m, a detailed examination of two-dimensional effects was not possible.

## PRESSURE BOUNDARY

The cavity pressure data obtained from CIST 20 were less than ideal. Two of the three gages fielded recorded data for long periods of time; however,

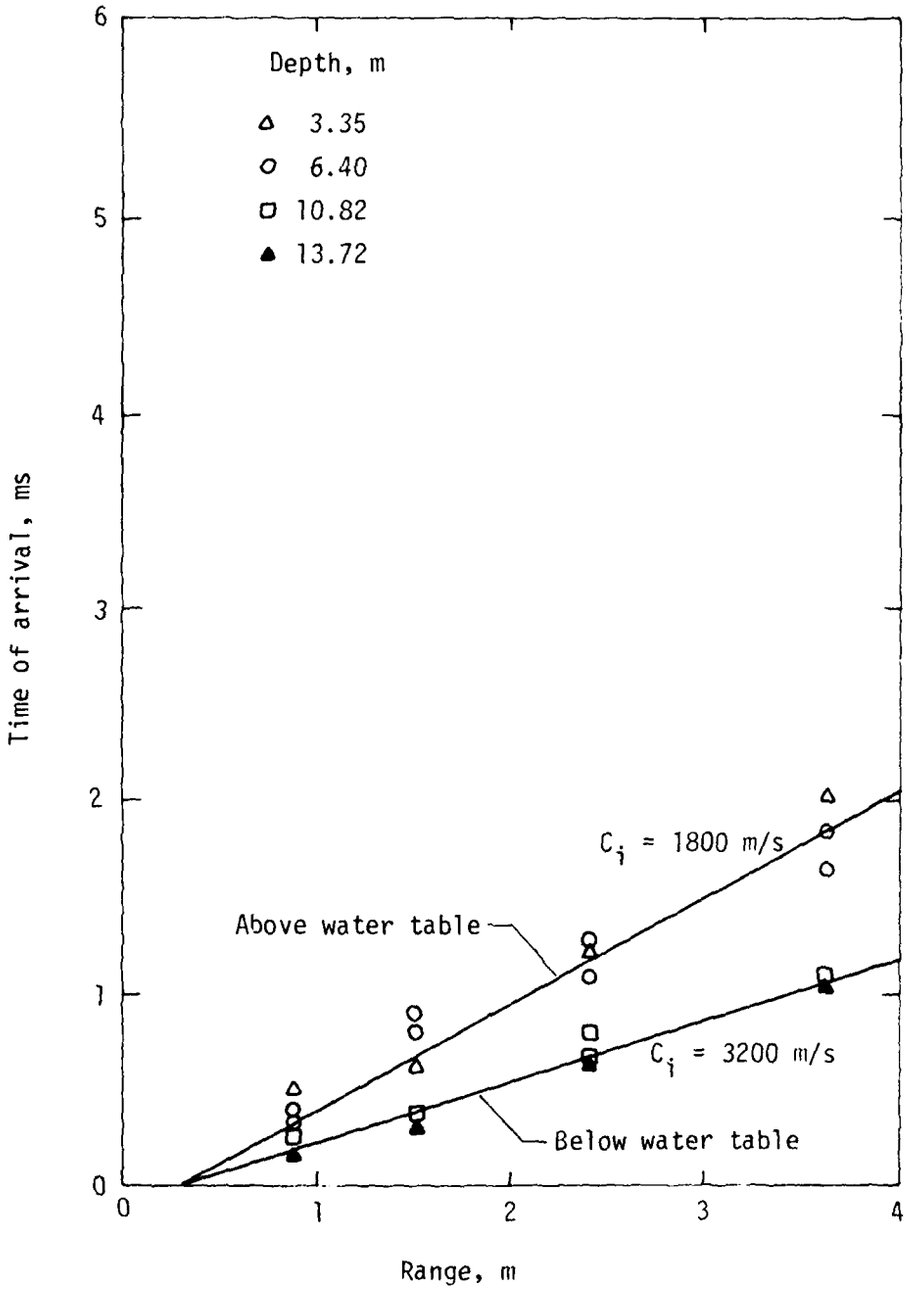


Figure 18. CIST 20 time of arrival.

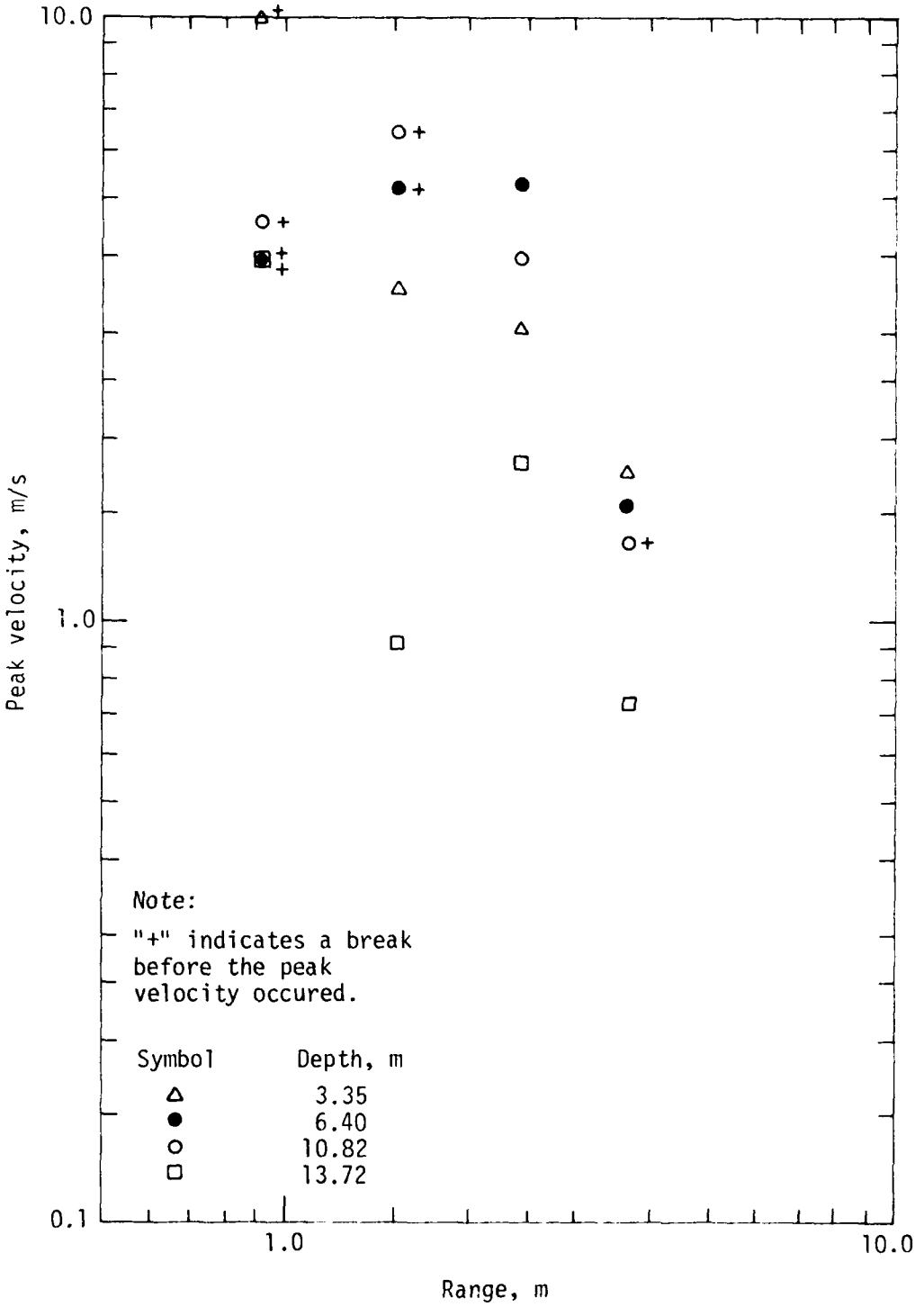


Figure 19. CIST 20 peak particle velocity versus range.

both gage records exhibited behavior different from what would be expected. Figures 20 and 21 are the records obtained at the 6.42- and 10.85-m depths respectively. In Figure 20 the -6.9 MPa (-1000 lb/in$^2$) initial pressure was believed to have been caused by case sensitivity in which stresses were locked in the case and consequently released by the pressure pulse resulting from detonation. In Figure 21 the long rise time makes the measurement suspect because a shock type detonation is usually recorded during CIST experiments. In the one-dimensional calculations for CIST 20 a pressure function of the type discussed earlier was used to approximate the data. The peak pressure was assumed to be 34.5 MPa (5000 lb/in$^2$) and the positive phase duration was assumed to be 0.125 s. The decay constant was determined to be N = 10. Thus the pressure function was

$$P(t) = 34.5 \left(1 - \frac{t}{0.125}\right)^{10} \qquad (3)$$

where

P(t) = pressure in megapascals

t = time in milliseconds

This relation has been plotted with the experimental data in Figures 20 and 21 for comparison. In Figure 21 the impulse from Equation 3 will be greater than the impulse from the experimental data. Equation 3 also seems to fit the experimental record of Figure 20, provided the assumed peak pressure of 34.5 MPa is valid. Equation 3 compares well with the relation used in the CIST 21 analysis.

## MATERIAL MODEL DEVELOPMENT

The initial hydrostat for CIST 20 was assumed similar to the CIST 21 hydrostat except in the low pressure region where the initial slope of the hydrostat was determined using the first time of arrival data, i.e., seismic wave speed, $C_i$. The initial failure surface was assumed to be the same as determined for CIST 21. The SPI code was used to obtain the model parameters which best fit the experimental records. The recommended model parameters are shown in Figure 22.

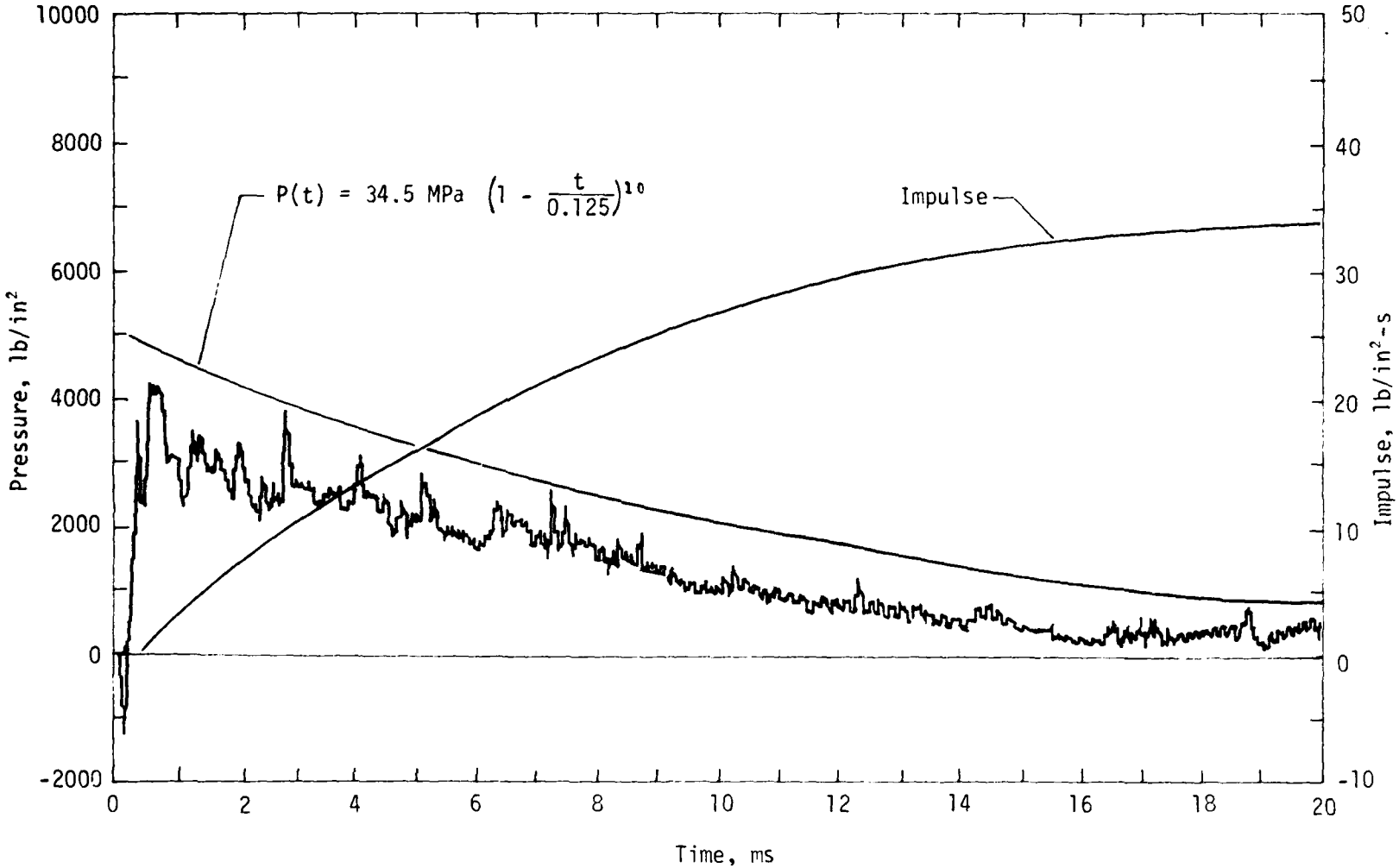


Figure 20. Comparison of experimental cavity pressure and functional fit used in calculations for CIST 20 at 6.42-m depth.

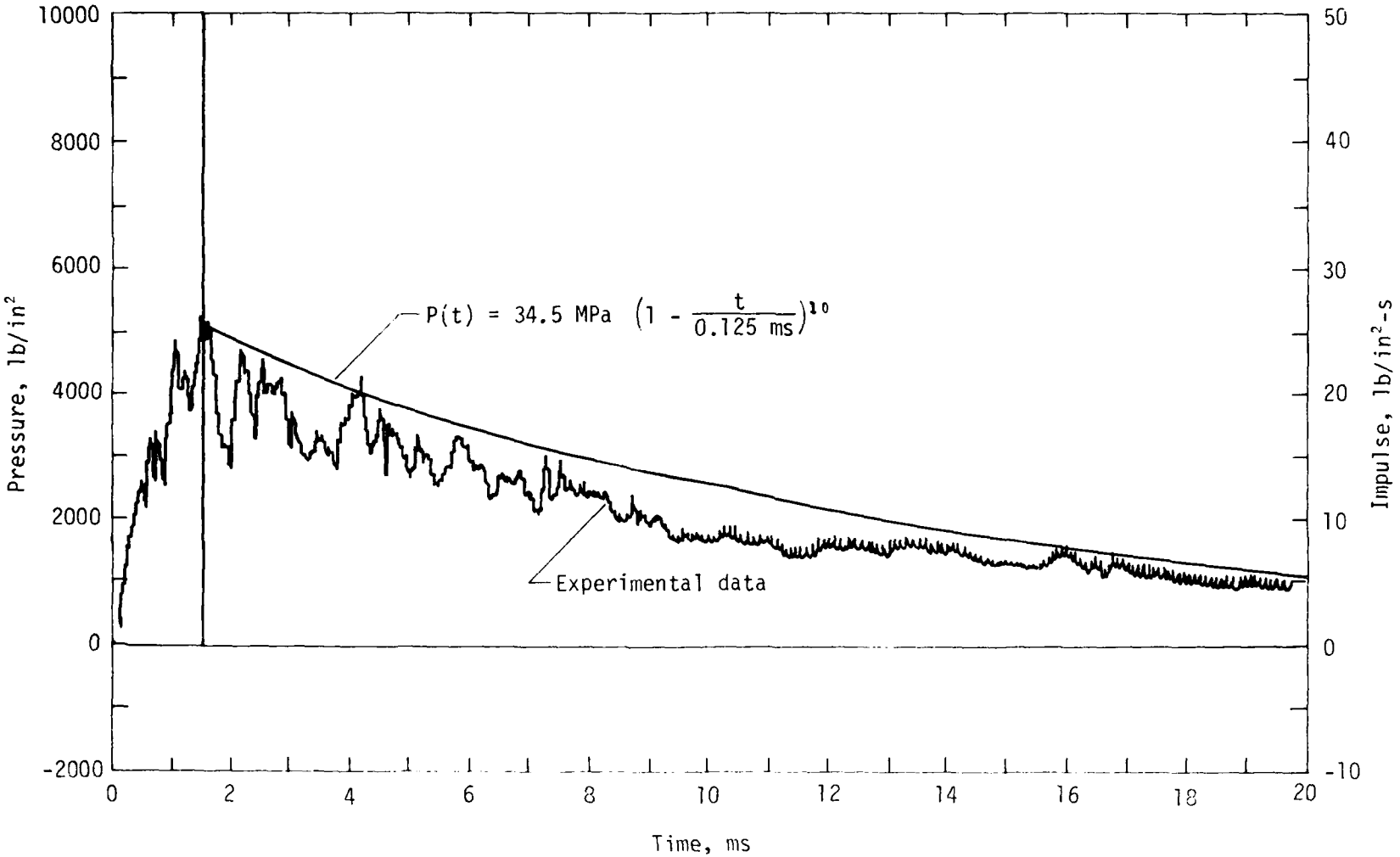


Figure 21. Comparison of experimental cavity pressure and functional fit used in calculations for CIST 20 at 10.85-m depth.

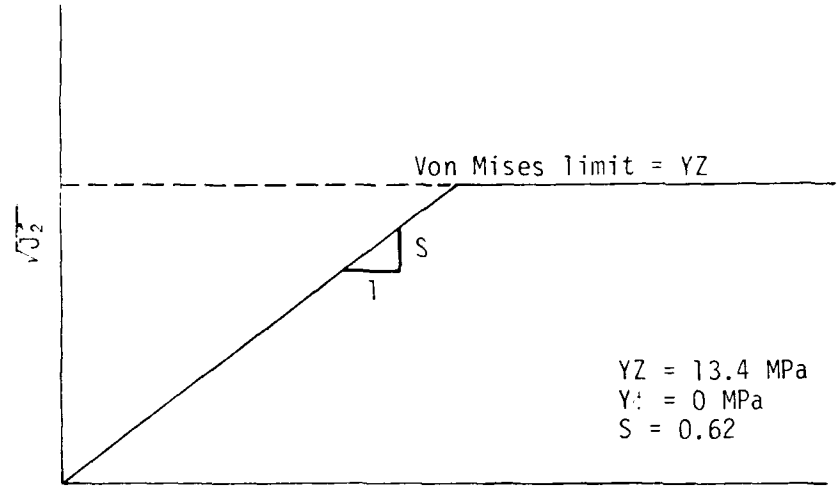


(a) Yield surface

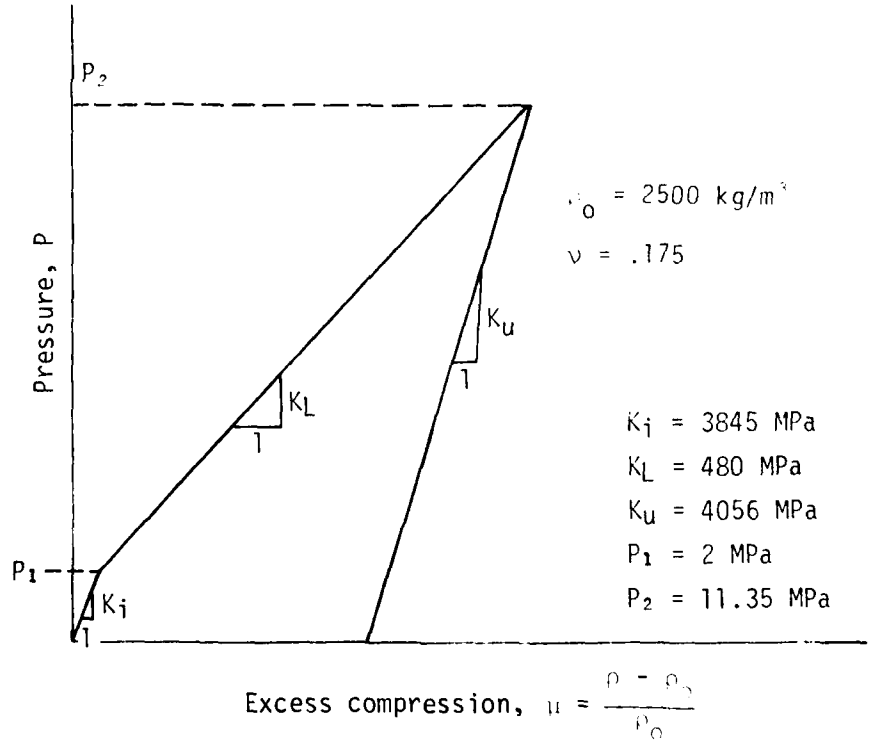


(b) Hydrostat

Figure 22. Recommended properties for CIST 20.

Figure 23 is a comparison of the experimental data obtained above the water table and the numerical waveforms calculated using the recommended material properties. The calculation is felt to be a reasonable match to both the 3.4- and the 6.4-m depths. At the 2.4-m range the calculated waveform falls below both of the experimental records, but an attempt to better match this range results in poor fits to the data at the other ranges. The 3.4- and 6.4-m depths were assumed to have identical properties; therefore deviations between data records represent variations which are unvoidable in in situ testing. These variations were not believed to be representative of significant material property changes within the material above the water table.

Figure 24 is a comparison of the experimental data from gages below the water table to the calculated waveforms using the recommended properties. As can be seen, the comparison is not very good. There are several problems that are significant in attempting to compare the experimental and calculated waveforms for the material below the water table. The first difficulty is that the data at the 13.71-m depth is near the bottom of the CIST cavity and two-dimensional effects may be dominating the motion records. Therefore comparing one-dimensional calculations to data with two-dimensional effects is meaningless.

At the 10.67-m depth there was only one record (R = 2.4 m) which survived for a significant period of the simulation time. On the basis of this single record it must be concluded that the material model obtained from the upper dry rhyolite does not predict the response of the rhyolite below the water table. Therefore additional analysis will be needed to obtain a model for saturated rhyolite. This analysis would have to be performed utilizing two-dimensional calculations and the data at the 13.7-m depth. By performing two-dimensional response calculations of CIST 20, the calculated vertical motion records could be compared with the experimental data. This may also determine if the model developed for rhyolite above the water table, using one-dimensional analysis, is valid for a two-dimensional calculation.

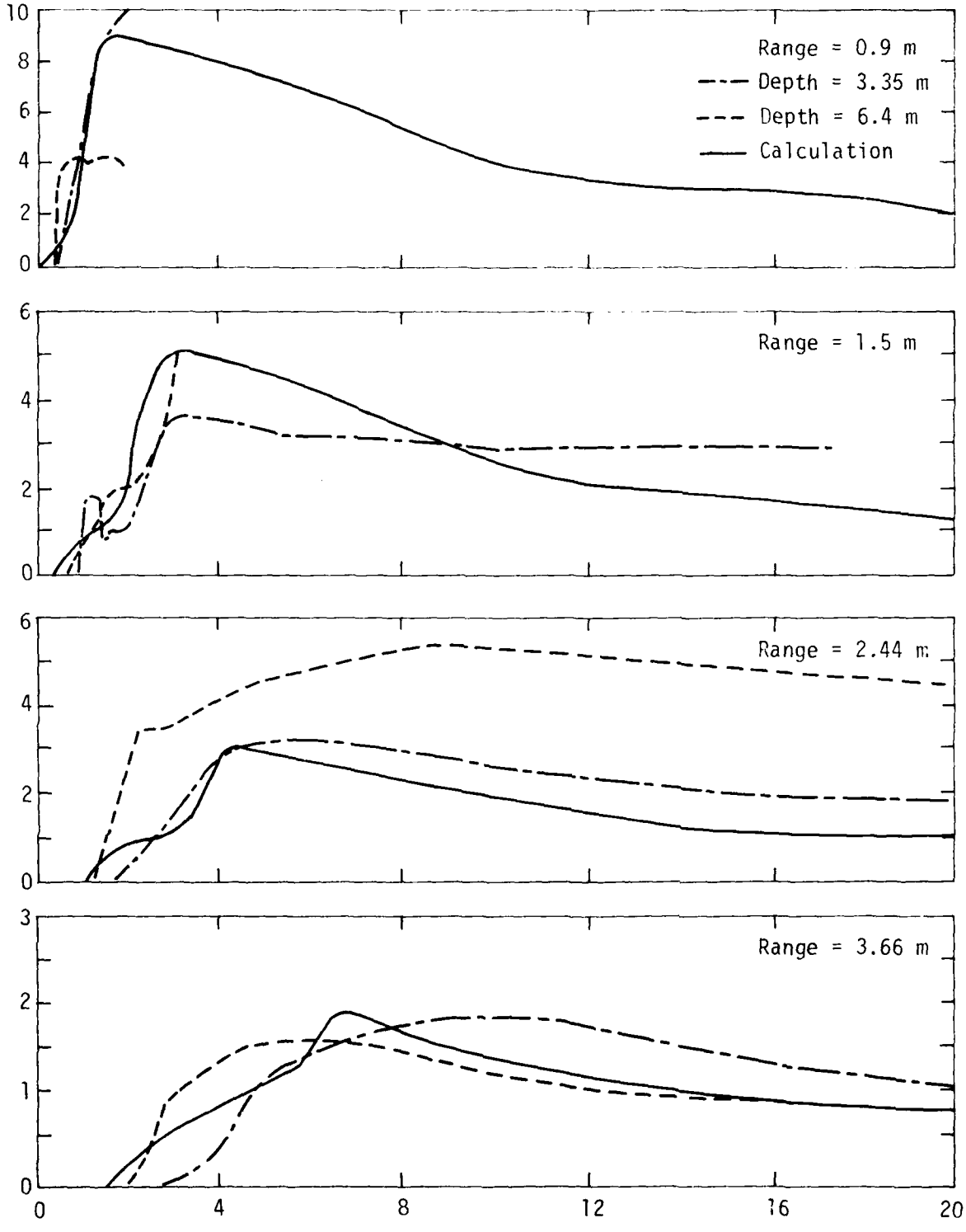


Figure 23. CIST 20: Comparison of experimental radial velocity waveforms and radial velocity waveforms from one-dimensional calculations for gages above water table.

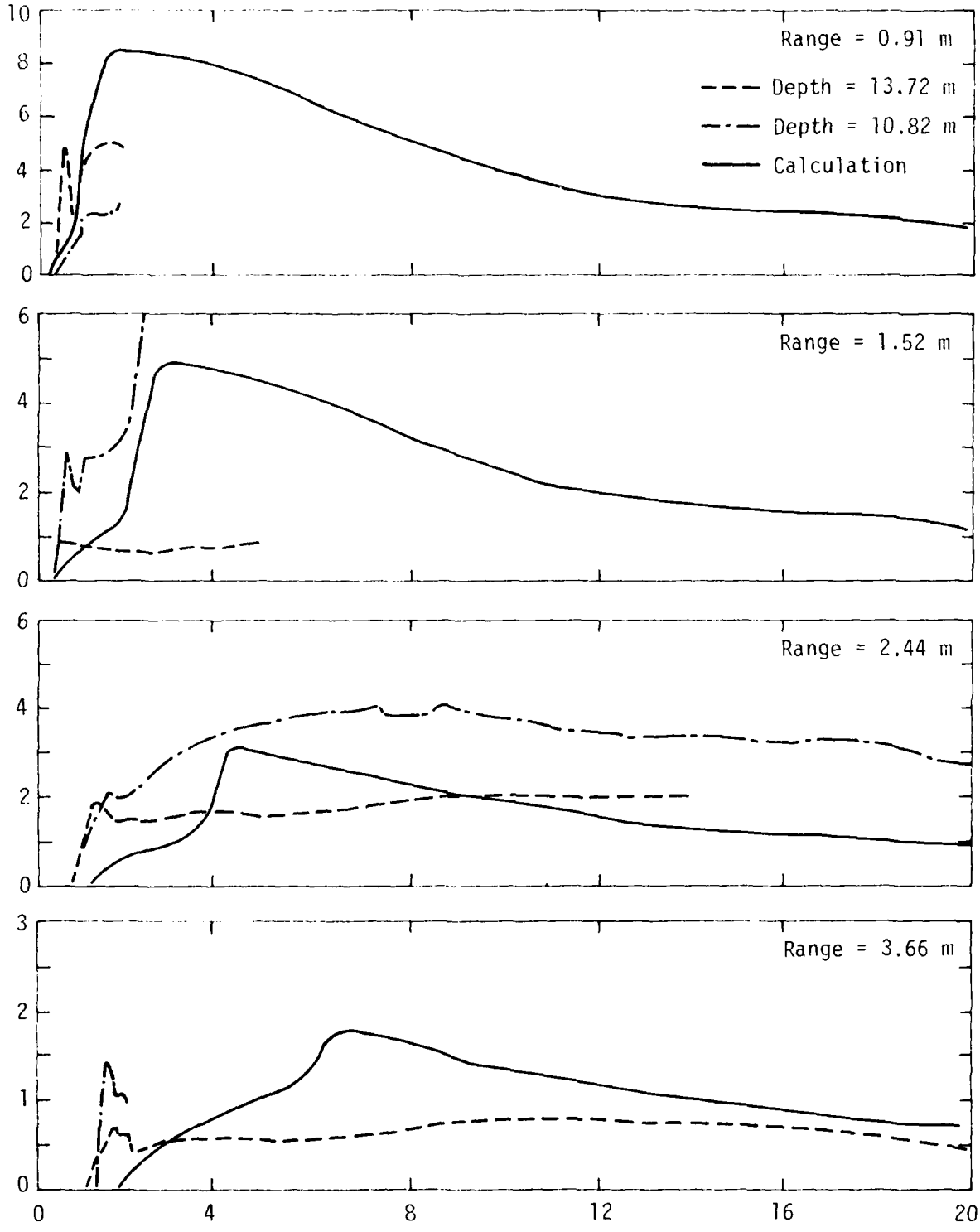


Figure 24. CIST 20: Comparison of experimental radial velocity waveforms and radial velocity waveforms from one-dimensional calculations for gages below water table.

# IV. COMPARISON OF LABORATORY AND IN SITU MATERIAL PARAMETERS

Tuff materials from Nevada have been studied extensively. Laboratory tests performed have included ultrasonic, uniaxial, and triaxial tests. Testing procedures generally consist of testing small intact samples which do not sufficiently represent the entire in situ material. In addition to laboratory testing some in situ seismic methods have been utilized.

In situ rock masses are seldom homogeneous. Fractures resulting from tectonic stresses, weathering, and shifting of rock masses are commonplace. Bedding planes and depositional characteristics also contribute to the nonhomogeneity of tuff. Brown and Swanson (Ref. 10) conducted triaxial tests on intact granite rock samples and specimens which were fractured in the laboratory. The fractured rock had lower strength at low confining pressures. However, at high confining pressures it behaved the same as the intact rock. In addition the axial stress-strain behavior of the fractured rock was more ductile than that of the intact rock. The same trends observed by Brown and Swanson should be evident in tuff although no laboratory tests have been performed on fractured tuff.

Sample disturbance will also influence the behavior of material tested in the laboratory. Tuff which was sampled at Mount Helen was found to have absorbed drilling water, resulting in an increase in water content of 1.5 to 8 percent (Ref. 11). It was also found that the ultrasonic wave velocities were 20 to 25 percent greater than in situ measured velocities. This would result in a uniaxial modulus which would be 1.6 to 2.4 times greater than the modulus determined from a seismic survey. Reference 11 recommends that the in situ modulus be used for the initial modulus, but offers no methodology for adjusting the higher stress moduli or failure surface to account for in situ conditions.

Because of the differences between laboratory and field conditions it is difficult to determine how laboratory tests can be used to develop material properties for field conditions. A field test such as CIST allows the evaluation of material properties hopefully with minimal disturbance at stress levels of interest.

Seismic surveys give only the elastic constants and may have little resemblance to the high stress properties. Stephens, Heurd and Schock (Ref. 12) suggest that for tuff the elastic sound waves travel through contact points between fractures and that the sound wave in effect finds a mean path through the fractures and cracks. Reference 5 also states that "The moduli (Bulk, Shear, Young's) below about 30 MPa are expected to be higher than either the in situ field or static (P-V) moduli, perhaps by as much as several hundred percent." This was due to the fracture and crack patterns. Reference 12 is concerned with high-pressure equations of state to 350 MPa. An expanded plot of their data in fact shows that the moduli is less than the initial modulus [Fig. 25 (Ref. 12)], but as the pores collapse the modulus increases. This is similar to the CIST 21 behavior and it may be expected that at higher pressure levels the tuff at the CIST 21 site would begin to stiffen as the cracks begin to close. Reference 12 also gives a good discussion on the effect of fracture on the shear strength of rocks.

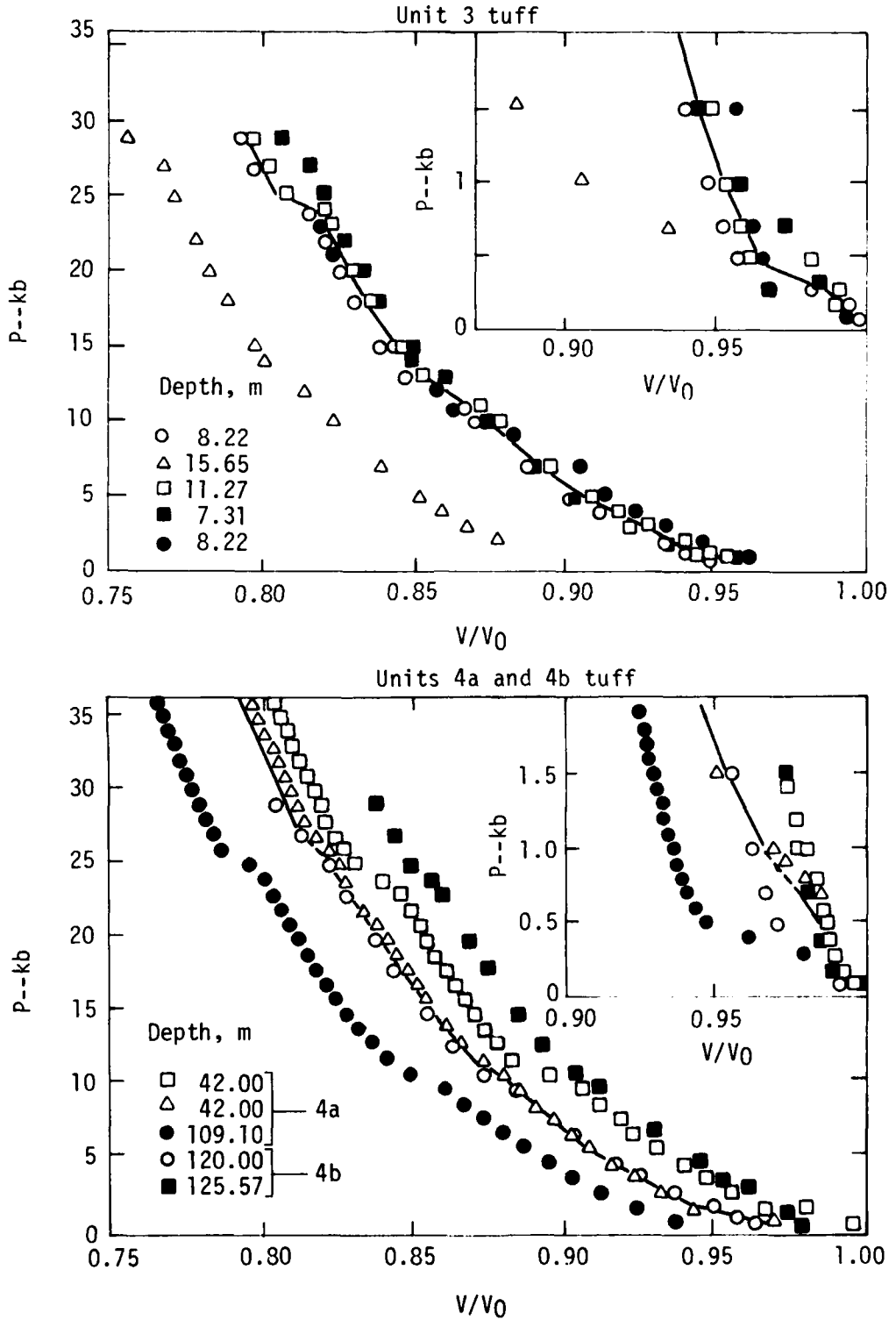


Figure 25. Loading P-V curves for Unit 3 tuff and Units 4a and 4b tuff.

# V. CONCLUSIONS

Material models were developed for tuff and rhyolite based on experimental data from CIST 21 and CIST 20 respectively. The CIST 21 tuff was found to be significantly stiffer than the rhyolite at CIST 20 although the in situ density of the rhyolite was greater. This was because the rhyolite was more highly fractured than the tuff. The failure surfaces suggested were similar with CIST 20 having a higher Von Mises limit. The recommended models for CIST 20 and CIST 21 could not match every detail of the experimental waveforms; however, they are an attempt to match the general character of the waveforms.

The major difference in modeling both CIST 20 and CIST 21 was that the behavior of the rhyolite located below the water table at CIST 20 could not be reproduced. In CIST 21 the tuff above and below the water table appeared to respond the same. This was felt to be due to the homogeneous nature of the tuff. The rhyolite below the water table responded differently from the dry rhyolite above the water table. In addition the loss of data below the water table in CIST 20 caused significant uncertainties in the analysis; therefore less effort was placed in analysis of that data. It was later learned that a borehole near the cavity had an elevated water level posttest. It is now believed that large excess pore pressures were generated during the CIST 20 event and that these pore pressures could have had a significant influence on the material model. It may be possible to develop a model for the material below the water table; however, the analysis will have to utilize two-dimensional calculations.

A survey was made of available publications regarding the properties of tuff from Nevada. In general, laboratory tests will overestimate the strength and stiffness of tuff because small intact samples tested in the laboratory are not representative of the in situ rock. The fracture pattern in situ cannot be tested in the laboratory, and these discontinuities are significant and to a large extent control the behavior of tuff and rhyolite in situ. It should be noted that CIST 20 and 21 were near-surface events and that the geostatic stresses are not believed to play a large role in material response. At greater depths the fractures may be less important.

To ensure adequate data recovery several changes to gage installation could be made. Armored cables could be used to ensure that the cables are not cut. In addition, exiting the cables from slanted holes would help improve data recovery. AFWL should investigate these and other techniques to improve the quality of data obtained from a CIST. Because of the very poor survival rate of blast pressure measurements, particular emphasis should be placed toward improving cavity pressure data recovery.

The CIST 20 and 21 tests provide a great deal of information and insight into the response of rock materials subjected to impulsive loadings. The material properties suggested are believed to be representative of the near-surface tuff; however, there are some unanswered questions regarding the behavior of saturated rhyolite at CIST 20.

For additional CIST 20 and CIST 21 related information, the reader is referred to Reference 13 which contains the experimental records for these events.

## REFERENCES


1. DiMaggio, F. L., and Sandler, I.S., "Material Model for Granular Soils," *Journal of the Engineering Mechanics Division, American Society of Civil Engineers*, Vol. 97, 1971.

2. Amend, J. H., III, Ullrich, G. W., and Thomas, J. M., *HAVE HOST Cylindrical In Situ Tests (CIST) Data Analysis and Material Model Report*, AFWL-TR-77-81, Air Force Weapons Laboratory, Kirtland Air Force Base, New Mexico, October 1977.

3. Lade, P. V., "Elasto-Plastic Stress-Strain Theory for Cohesionless Soil with Curved Yield Surface," *International Journal of Solids Structures*, Vol. 13, p. 1019, 1977.

4. Prevost, J. H., "Plasticity Theory for Soil Stress Strain Behavior," *Journal of Engineering Mechanics Division, American Society of Civil Engineers*, Vol. 104, p. 1177, October 1978.

5. Valanis, K. C., and Read, H. E., *A New Endochronic Plasticity Theory for Soils*, SSS-R-80-4294, Systems, Science and Software, La Jolla, California.

6. Read, H. E., *Evaluation of Material Models for MX Siting, Volume II: Soils Models*, SSS-R-80-4255, Systems, Science and Software, La Jolla, California, November 1979.

7. Fedock, J. J., Higgins, C. J., and Bratton, J. L., *Effects of Material Properties on Cylindrical Wave Propagation in Geologic Materials*, AFWL-TR-77-184, Air Force Weapons Laboratory, Kirtland Air Force Base, New Mexico, October 1978.

8. Kovarna, J., *An Interim Guide To the Use of the CERF SPI Code*, report prepared by the Civil Engineering Research Facility, University of New Mexico, for Air Force Weapons Laboratory, Albuquerque, New Mexico, July 1978.

9. Lawrence, R. J., and Mason, D. S., *WONDY IV--A Computer Program for One-Dimensional Wave Propagation with Rezoning*, SC-RR-710284, Sandia Laboratories, Albuquerque, New Mexico, October 1971.

10. Brown, W. S., and Swanson, S. R., *Constitutive Equations for Westerly Granite and Cedar City Tonalite for a Variety of Loading Conditions*, DASA 2473, March 1970.

11. Butter, S. W., Swolfs, H. S., Johnson, J. M., Butler, D., and Hadala, P. F., *Field, Laboratory and Modeling Studies on Mount Helen Welded Tuff for Earth Penetrator Test Evaluation*, DNA 4085F, August 1976.

12. Stephens, D. R., Heard, H. C., and Schock, R. N., *High Pressure Mechanical Properties of Tuff from the Diamond Dust Site*, UCRL-50858, April 22, 1970.

13. Amend, J., and Brown, R., *Cylindrical Impact Tests at Selected Test Sites*, AFWL-TR-79-61, Air Force Weapons Laboratory, Kirtland Air Force Base, New Mexico, August 1980.

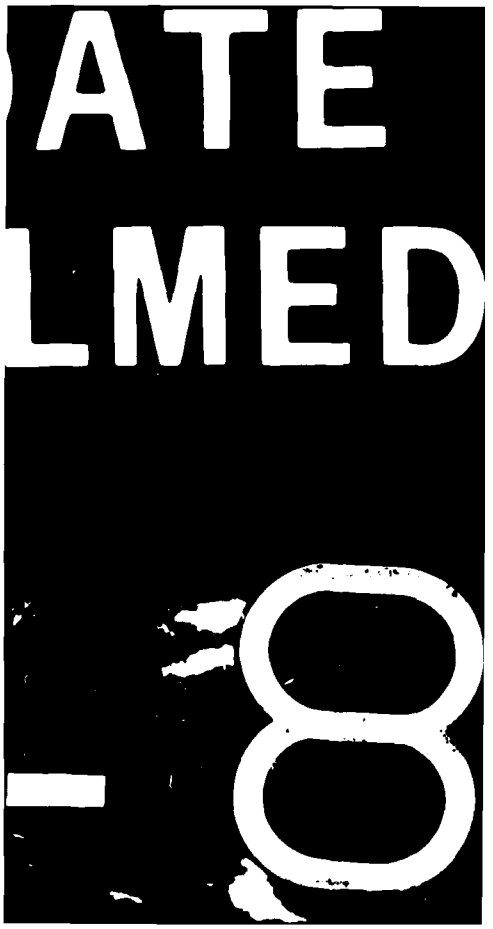
ATE
LMED
-8